AGU PUBLICATIONS

JGR

Journal of Geophysical Research: Oceans

RESEARCH ARTICLE

10.1002/2017JC013174

The Effect of Alongcoast Advection on Pacific Northwest Shelf and Slope Water Properties in Relation to Upwelling Variability

Hally B. Stone[1], **Neil S. Banas**[2], **and Parker MacCready**[1]

[1]School of Oceanography, University of Washington, Seattle, Washington, USA, [2]Department of Mathematics and Statistics, University of Strathclyde, Glasgow, UK

Key Points:
- Midshelf bottom water properties tend to vary across isopycnals, while upper slope water properties tend to vary along isopycnals
- The origins of both midshelf bottom water and upper slope water are affected by large-scale alongcoast advection
- Upwelling variability is more important to shelf water oxygen and DIC than alongcoast advection, except during anomalous years

Correspondence to:
H. B. Stone,
hbstone@uw.edu

Citation:
Stone, H. B., Banas, N. S., & MacCready, P. (2018). The effect of alongcoast advection on Pacific Northwest shelf and slope water properties in relation to upwelling variability. *Journal of Geophysical Research: Oceans*, *123*. https://doi.org/10.1002/2017JC013174

Received 6 JUN 2017
Accepted 12 DEC 2017
Accepted article online 28 DEC 2017

Abstract The Northern California Current System experiences highly variable seasonal upwelling in addition to larger basin-scale variability, both of which can significantly affect its water chemistry. Salinity and temperature fields from a 7 year ROMS hindcast model of this region (43°N–50°N), along with extensive particle tracking, were used to study interannual variability in water properties over both the upper slope and the midshelf bottom. Variation in slope water properties was an order of magnitude smaller than on the shelf. Furthermore, the primary relationship between temperature and salinity anomalies in midshelf bottom water consisted of variation in density (cold/salty versus warm/fresh), nearly orthogonal to the anomalies along density levels (cold/fresh versus warm/salty) observed on the upper slope. These midshelf anomalies were well-explained ($R^2 = 0.6$) by the combination of interannual variability in local and remote alongshore wind stress, and depth of the California Undercurrent (CUC) core. Lagrangian analysis of upper slope and midshelf bottom water shows that both are affected simultaneously by large-scale alongcoast advection of water through the northern and southern boundaries. The amplitude of anomalies in bottom oxygen and dissolved inorganic carbon (DIC) on the shelf associated with upwelling variability are larger than those associated with typical variation in alongcoast advection, and are comparable to observed anomalies in this region. However, a large northern intrusion event in 2004 illustrates that particular, large-scale alongcoast advection anomalies can be just as effective as upwelling variability in changing shelf water properties on the interannual scale.

1. Introduction

In eastern boundary current upwelling systems like the California Current System (CCS), upwelled water is a significant source of nutrients for organisms on the continental shelf (e.g., Hickey & Banas, 2003; MacFadyen et al., 2008). Water upwelled onto CCS shelves is derived from the California Undercurrent (CUC), a warm, salty, low-oxygen, high-inorganic carbon, and high-nutrient poleward current (Hickey, 1979; MacFadyen et al., 2008; Pierce et al., 2000; Thomson & Krassovski, 2010). Changes in the equatorial source waters of the CUC have been suggested to drive long-term trends in the composition of water upwelling onto the shelf in the CCS (Bograd et al., 2015; Meinvielle & Johnson, 2013). At the same time, a number of processes on regional and local scales have been observed or hypothesized to drive interannual variability in the water supplied to the shelf by upwelling, from local and remote wind-driven dynamics (e.g., Battisti & Hickey, 1984; Connolly et al., 2014; Hickey et al., 2006, 2016) to large-scale alongcoast advection (e.g., Freeland et al., 2003; Kosro, 2003). This study uses a 7 year ROMS model hindcast to directly compare the effects of these processes in the Northern CCS (north of 42°N; NCCS): in particular, the effect of variability in the depth and composition of the CUC and in alongcoast advection on midshelf bottom water properties, in comparison with local and remote wind forcing, as well as an estimation of how these mechanisms may impact midshelf bottom water chemistry.

1.1. Northern California Current System

Large-scale circulation in the NCCS includes the California Current, the California Undercurrent, and the wintertime Davidson Current (Hickey, 1979). The California Current is an equatorward surface current, present year-round, that extends seaward about 1,000 km from the shelf break. It is strongest at the surface, with a mean velocity of 10 cm s^{-1}, and offshore, it extends to about 500 m depth, and within 300 km of the coast, it extends to about 150 m (Hickey, 1979, 1989). The California Undercurrent (CUC) is a seasonal narrow

(usually 10–20 km wide) subsurface current that flows poleward over the upper slope (core ~ 250 m depth) with mean poleward velocities of ~10 cm s^{-1}, which strengthens over the upwelling season (Hickey, 1979; Pierce et al., 2000; Thomson & Krassovski, 2010).

In the NCCS, upwelling, driven by equatorward alongshore winds, typically occurs during the summer into the fall and downwelling, driven by poleward alongshore winds, occurs in winter. Event-scale (several days) upwelling and downwelling can occur within each season. Both local and remote wind forcing drive upwelling and downwelling, with remote wind (alongshore winds at and south of about 42°N) forcing playing a large role in upwelling due to the relatively weak local winds in the NCCS (Battisti & Hickey, 1984; Connolly et al., 2014; Hickey & Banas, 2003; Hickey et al., 2006, 2016). In particular, Battisti and Hickey (1984) show that off of Washington during the summer, over 35% of the energy in alongshelf currents generated from remote forcing originates between Cape Mendocino (40.4°N) and San Francisco, California (37.8°N), with the most energetic wind found at 39°N.

During the upwelling season, equatorward winds drive Ekman transport offshore in the upper 10–30 m, and equatorward flow develops over the shelf (Hickey, 1989; Lentz, 1992). The water column interior experiences equatorward flow over much of the shelf, with poleward flow developing at depth over the outer shelf and midshelf as the upwelling season progresses (Hickey, 1989). The onshore return flow, compensating the offshore flow at the surface, occurs higher in the water column as the season progresses, while in the bottom boundary layer (bottom 5–15 m), flow is onshore in the beginning of the upwelling season, and weakens and transitions to offshore flow later in the season (Hickey, 1989; McCabe et al., 2015). This change in the direction of cross-shelf flow is a consequence of changing the sea level gradient from equatorward (lower sea level in the south) to poleward (higher sea level in the south; McCabe et al., 2015). During the downwelling season, alongshore flow over the shelf is poleward. Northward winds push the surface Ekman transport onshore, while flow in the bottom boundary layer is offshore (Hickey, 1989).

Hickey et al. (2016) provides a thorough analysis of interannual variability and alongcoast structure of measured midshelf water properties in the NCCS from a suite of moored sensors deployed from 2000 to 2006. Results showed that while winter subsurface water properties on the shelf were strongly correlated with local winds, summer water properties were more strongly correlated with remote winds. Furthermore, Hickey et al. (2016) found that the alongcoast wind gradient can drive variability within the NCCS upwelling system. In particular, they link the unusually warm and fresh summer water properties observed in 2004 to the loss of the alongcoast wind gradient that year, as well as weaker remote and local winds, resulting in a shallower, warmer, and fresher CUC. The upwelling regime is further complicated by variable bathymetry, with enhanced upwelling through canyons, particularly in the northern-most portions of the NCCS (Alford & MacCready, 2014; Connolly & Hickey, 2014; Hickey, 1997).

1.2. California Undercurrent

As shown in previous studies (e.g., Hickey, 1979; Pierce et al., 2000; Thomson & Krassovski, 2010), the CUC is a seasonal feature of the CCS, flowing over the continental slope between 150 and 300 m depth. The CUC originates in the equatorial Pacific, thus carrying with it warm and salty Pacific Equatorial Water (PEW; Hickey, 1979; Pierce et al., 2000; Thomson & Krassovski, 2010). Thomson and Krassovski (2010) tracked the poleward extension of the CUC over several decades and found that in the NCCS it contains about 35–40% PEW. The CUC develops at the onset of the upwelling season, strengthening through the summer into the fall (Hickey, 1979). Once the winds transition to downwelling favorable in the winter, the CUC shoals and is replaced by or becomes the Davidson Current, the surface-intensified poleward flow over the slope (Hickey, 1979). The CUC is affected by coastal-trapped waves, which are driven by remote winds, the baroclinic component of the alongshore pressure gradient force, and sea level variability south of the NCCS (Connolly et al., 2014).

Variability in the CUC manifests in its depth, strength, and composition. In addition to its seasonal movement in the water column, the vertical position of the CUC has interannual and latitudinal variation (Thomson & Krassovski, 2010). The CUC's composition can change as it flows poleward losing heat and salt, the components of PEW, through along-isopycnal stirring in part due to anticyclonic eddies (cuddies) at CUC depth (Pelland et al., 2013; Pierce et al., 2000; Thomson & Krassovski, 2010). The composition can also vary interannually, such as the slightly fresher composition of the CUC observed in 2004 (Hickey et al., 2016).

1.3. Alongcoast Advection

Variability in large-scale alongcoast advection may drive water property variability in the NCCS. Typically, water that upwells onto the shelf is from the CUC, which carries PEW from the south (e.g., MacFadyen et al., 2008), though the source depth of water upwelled onto the shelf can vary both seasonally (typically shoaling throughout the upwelling season) and interannually (e.g., Chhak & Di Lorenzo, 2007; Di Lorenzo et al., 2008; Jacox et al., 2015; Peterson et al., 2013). However, occasional intrusions of subarctic water from the north onto the shelf in the NCCS have also been observed, bringing water that is colder and fresher than the typical summertime properties (Freeland et al., 2003; Grantham et al., 2004; Huyer, 2003; Kosro, 2003). Variations in transport on this scale are at least in part linked to modes of ocean-climate decadal variability, such as the North Pacific Gyre Oscillation (NPGO) and Pacific Decadal Oscillation (PDO). The NPGO is correlated with geostrophic transport in the North Pacific Current (Di Lorenzo et al., 2009), and Peterson et al. (2013) found the NPGO is a particularly strong predictor of hypoxia in the NCCS, attributing this link to changes in advection. The PDO is also correlated with anomalies in alongcoast advection that bring subarctic copepod communities into the NCCS during negative-PDO years and subtropical copepod communities during positive-PDO years (Keister et al., 2011), though a similar relationship between PDO and hypoxia in the NCCS was not found (Peterson et al., 2013).

This paper uses a comprehensive regional model of the NCCS developed by the University of Washington Coastal Modeling Group to investigate the effect of variability in the depth and composition of the CUC and in alongcoast advection from the north and south on midshelf bottom water properties. This model has been well validated with an extensive, multiyear observational data set as part of the PNWTOX (Pacific Northwest Toxins) study (Davis et al., 2014; Giddings et al., 2014; Siedlecki et al., 2015). Compared to the recent observational study of interannual variability in midshelf water properties described in Hickey et al. (2016), the advantages of using a model to study water property variability is that both of the upper slope and shelf are sampled, the spatial resolution is higher, with 1.5 km resolution over the slope and shelf, and the model covers a somewhat longer time period (2003–2009). We will first use an Eulerian analysis to characterize variability in midshelf bottom water properties and CUC depth and composition, and then use Lagrangian analysis to characterize variability in water origin on the upper slope and adjacent shelf. Lastly, using mean oxygen and dissolved inorganic carbon (DIC) fields from other studies, we will extrapolate our findings to infer how variability in CUC depth and in alongcoast advection may affect oxygen and DIC variability in this region.

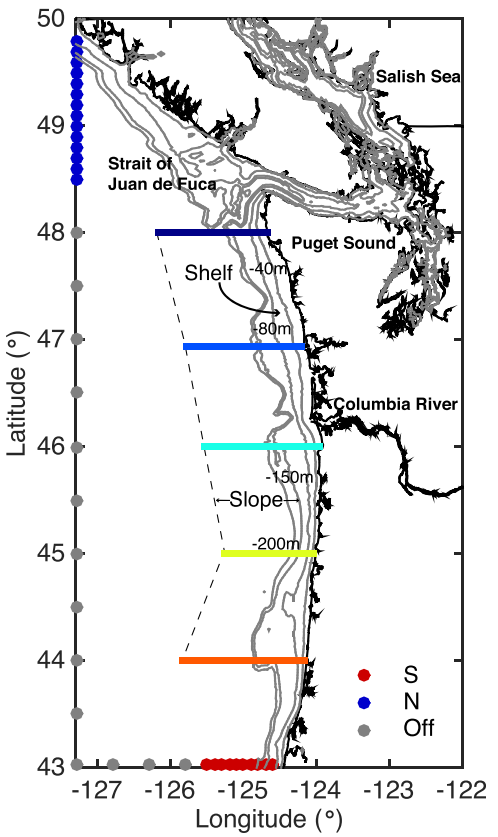

Figure 1. Model domain and particle tracking release points. Colored lines indicate latitudes where gridded analysis was conducted. Dots indicate particle release points and are colored by origin, with northern (N) particles in blue, southern (S) particles in red, and offshore (Off) particles in grey. Also plotted in grey are the 40, 80, 150, and 200 m isobaths. The "shelf" (between 40 and 80 m isobaths) and "slope" (between 150 m isobath and 1° longitude offshore of the 150 m isobath) regions are indicated on the figure, along with geographical regions described in the text.

2. Methods

2.1. Model Description and Validation

For this study, we used the Cascadia model developed by the University of Washington Coastal Modeling Group (Giddings et al., 2014; Sutherland et al., 2011). The model was implemented using Regional Ocean Modeling System (ROMS; Shchepetkin & McWilliams, 2005), a free surface, hydrostatic, primitive equation model. The model domain (Figure 1) includes the Salish Sea and coastal ocean of Washington, northern Oregon, and southern British Columbia. The horizontal resolution of the model is 1.5 km over shelf and slope, expanding out to a maximum of 4.5 km offshore. Vertically, the model has 40 *S*-coordinate layers with stretching parameters set to better resolve the near-bottom and the upper water column. Ocean initial state and forcing on the southern and western boundaries were taken from the global Navy Coastal Ocean Model (NCOM; Barron et al., 2006, 2007). Tides were specified by the quarter-degree TPXO7.2 inverse global tidal model (Egbert & Erofeeva, 2002). Rivers were forced by daily discharge

data from the Columbia River, Fraser River, and 14 Puget Sound rivers using data from the USGS and Environment Canada (Giddings et al., 2014). All atmospheric forcing was derived from the fifth-generation Mesoscale Model (MM5) from Pennsylvania State University—National Center for Atmospheric Research (transitioning to the Weather Research and Forecasting model (WRF) in April 2008) regional atmospheric forecast model (Mass et al., 2003).

Giddings et al. (2014) used observational data to validate the physical model on event to seasonal scales. Overall, the model's temperature, salinity, and sea surface elevation had high Willmott Skill Scores ($WS \geq 0.92$; Willmott, 1982), based on comparison with data from 2,264 CTD casts in 2005. Comparisons of satellite images with monthly sea surface temperature model fields showed that spatial patterns associated with coastal upwelling and downwelling are well represented by the model. Additionally, comparison of velocity structure over the shelf between moored sensor data at selected sites and the model showed that coastal-trapped waves, an important feature in this region, are well captured, with the expected event-scale variability associated with coastal-trapped waves evident in along-stream velocity at both the surface ($WS = 0.85$; correlation coefficient (R) = 0.75) and at 30 m depth ($WS = 0.86$; $R = 0.83$). Comparison of density and velocity data from 20 glider cross-sections spanning 2005–2007 with model data showed that the location, magnitude, and seasonal variability of the model's CUC was in good qualitative agreement with observations, with the model consistently producing the CUC, with similar magnitude, location, and seasonal development as found in observations. The model's skill decreases beyond the shelf break where it is poorly constrained due to sparse data. Additionally, there is insufficient mixing within the Salish Sea and Strait of Juan de Fuca, likely because the model is unable to resolve their extreme bathymetry, leading to warmer (~2°C) summer temperatures in the Juan de Fuca eddy and Strait of Juan de Fuca, though this bias is confined to the top ~20 m. Also, there is a deep salinity bias in the model (about 0.2 psu) that is inherited from NCOM boundary conditions (Giddings et al., 2014). More detailed validation, including specific model skill metrics, and further model description can be found in Giddings et al. (2014). The Cascadia model also includes a coupled biogeochemical model (Davis et al., 2014; Siedlecki et al., 2015) that has demonstrated significant skill at predicting nutrients (nitrate concentrations, $WS = 0.93$) and oxygen (oxygen concentrations, WS (2006) = 0.81, WS (2007) = 0.91) fluctuations on event to seasonal scales—a further indirect validation of the model physics—although the biogeochemical model is not used here because it was run for a more limited range of years.

2.2. Eulerian Analysis

A hindcast of physical parameters, including temperature, salinity, and velocity, spanning 2002–2009 was produced using the Cascadia model. Each individual year 2002–2009 was run in ROMS initialized from NCOM, and then each year 2003–2009 was re-run initialized from the previous year's ROMS run. The year 2002 was thus discarded as spin-up. The hourly output of the Cascadia model was low-pass filtered to daily values (Godin low-pass filter; Emery & Thomson, 2004). Depth-longitude slices of salinity (S) and potential temperature (θ) were extracted along each latitude from 44°N to 48°N for each year spanning 2003–2009. A 30 day Hanning filter was then applied to these data, resulting in monthly values, for each of the depth-longitude slices. In this study, we use the monthly values obtained from the 30 day Hanning filter as monthly means. To capture midshelf bottom water, the mean was obtained over the bottom 8 S-layers of the model domain between 40 and 80 m isobaths at each latitude slice. These depth intervals correspond to ~10 m above bottom at the 80 m isobath tapering down to ~5 m above bottom at the 40 m isobath (Figure 2a). We will refer to this section of the midshelf bottom as the "shelf" for the remainder of this paper.

To capture CUC water, whose core depth changes both seasonally (Hickey, 1979) and with latitude (Thomson & Krassovski, 2010), model output was interpolated first onto a z-position grid (−3,000 to 0 m, with 10 m intervals) and then onto a σ_t grid (15–30 kg m^{-3}, with 0.05 kg m^{-3} intervals). Then, an upper slope water box was defined as from the 150 m isobath to 1° longitude offshore of the 150 m isobath (western boundary ranging from 125.5°W to 126.5°W, depending on latitude; Figure 1), and from $\sigma_t = 26.25$ to 27.0 kg m^{-3} (Figure 2b). This definition is based on Thomson and Krassovski (2010) (see Figure 2 in Thomson and Krassovski (2010)). We will refer to this section of the upper slope as the "slope" for the remainder of the paper. As with the shelf water, the mean was taken over this slope water box, yielding time series at each latitude (44°N–48°N), spanning 2003–2009, of potential temperature (θ), salinity (S), fraction of Pacific Equatorial Water (f_{PEW}), and z-position of the $\sigma_t = 26.5$ kg m^{-3} isopycnal ($z_{26.5}$), representing the depth of

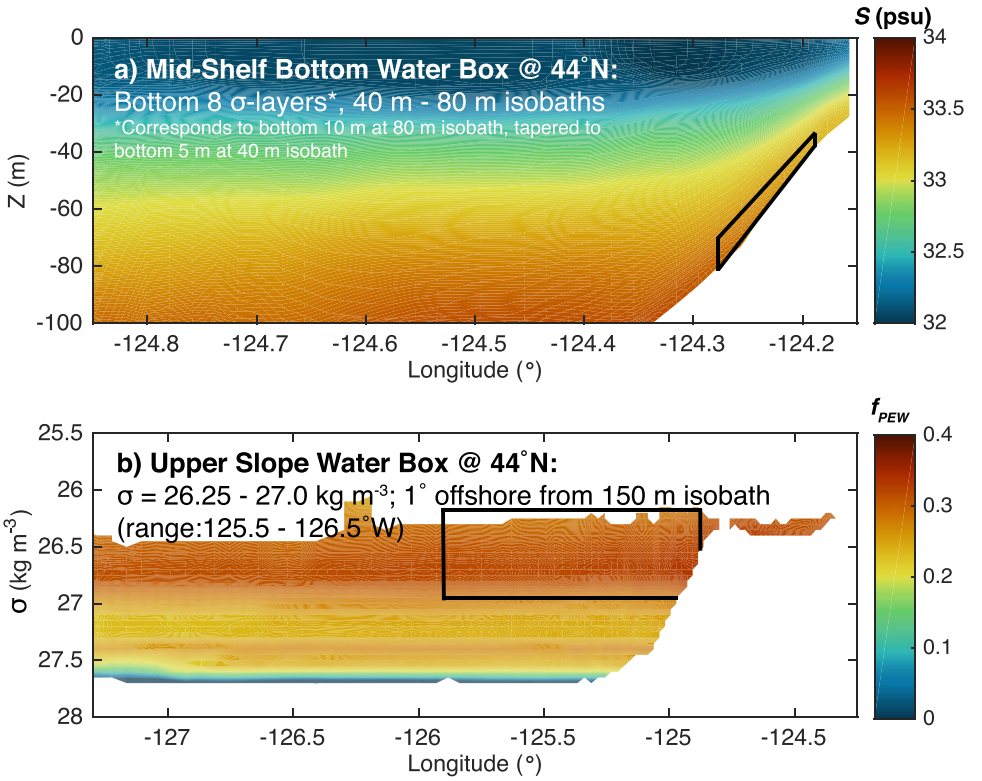

Figure 2. Example of (a) midshelf bottom water at 44°N and (b) upper slope water definitions at 44°N. The midshelf bottom water box encompasses the bottom 8 *S*-layers in the model between 40 and 80 m isobaths, corresponding to 10 m above the 80 m isobath and 5 m above the 40 m isobath, and this definition is depicted on top of salinity contours (*S*; psu). The upper slope water box is based on density and spans $\sigma_t = 26.25–27.0$ kg m^{-3}, from the 150 m isobath to 1° longitude offshore of the 150 m isobath (varies with latitude, ranging from 125.5°W to 126.5°W; z∼100 km), and this definition is depicted on top of fraction of Pacific Equatorial Water (f_{PEW}) contours. In this paper, "shelf" refers to the midshelf bottom definition and "slope" refers to the upper slope definition.

the CUC core in the water column. However, if the overall composition of the CUC changes so that its core lies above the $\sigma_t = 26.5$ kg m^{-3} isopycnal, which happened in 2004 (Hickey et al., 2016), then $z_{26.5}$ would not represent the depth of the CUC core. The convention for $z_{26.5}$ is that positive changes in its position indicate a movement upward in the water column. The f_{PEW} in the slope water was calculated by interpolation along isopycnals between the Pacific Equatorial Water (PEW) and Pacific Subarctic Upper Water (PSUW) end-members defined by Thomson and Krassovski (2010). Note that due to modification of water properties by freshwater input, surface heating, and local mixing processes, f_{PEW} on the shelf falls outside the temperature-salinity curves of the PEW and PSUW definition (Thomson & Krassovski, 2010), precluding its use in shelf water analysis. In the analysis below, we thus compare f_{PEW} on the slope with salinity on the shelf (S_{shelf}).

Interannual anomalies were calculated from each of these time series by removing the seasonal cycle (monthly means) of each property on the shelf and slope. Mean seasonal cycles of salinity and temperature on the shelf and slope (Figure 3) are consistent with observed seasonal cycles, with cold, salty water present on the shelf (Figures 3a and 3c) during the upwelling season (e.g., Hickey, 1989; Hickey et al., 2016; Huyer, 1977), though the shelf water is fresher in the model than in observations (about 0.5 psu) due to the salinity bias inherited from NCOM (Giddings et al., 2014), as well as differences between measurement locations in observations and method of averaging with the model output. There was a smaller seasonal cycle in slope water salinity and temperature, with slightly colder and fresher water during the upwelling season. While the expected trend of warmer and saltier slope water during the upwelling season (due to PEW present over the slope; e.g., Hickey, 1979; Pierce et al., 2000; Thomson & Krassovski, 2010) is not evident in the model, this departure is likely due to the method of capturing the CUC by density rather than by depth, resulting in a slope water box with a constant density and seasonal variability in its vertical position.

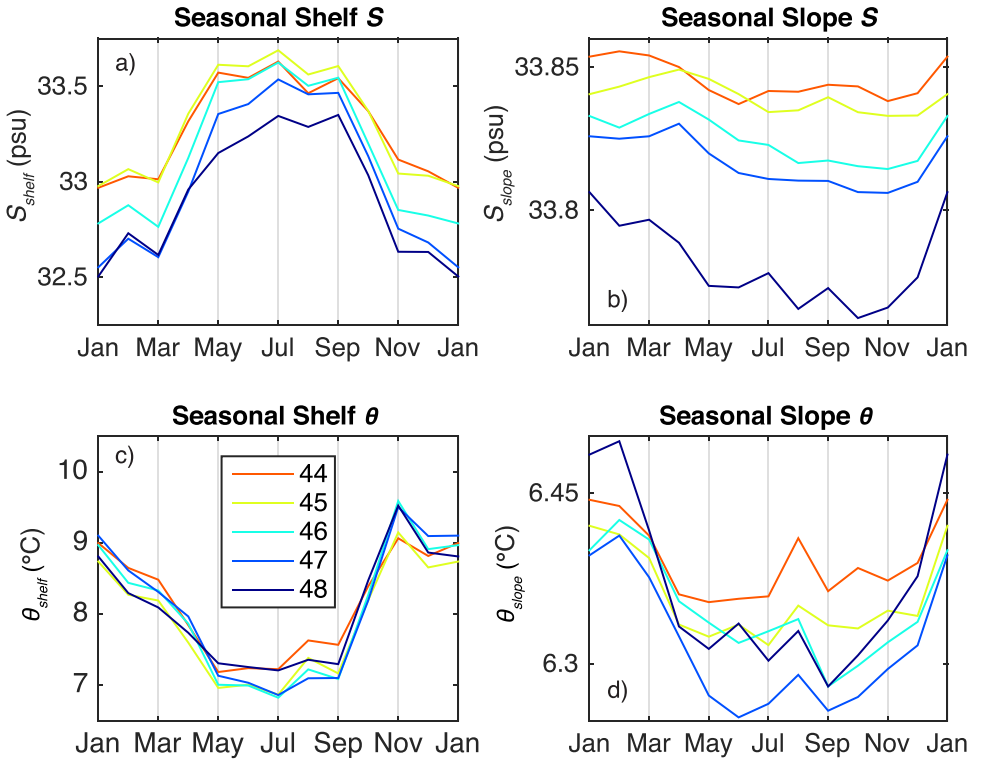

Figure 3. Seasonal salinity for the (a) shelf (S_{shelf}; psu) and (b) slope (S_{slope}; psu), and seasonal temperature for the (c) shelf (θ_{shelf}; °C) and (d) slope (θ_{slope}; °C) with color denoting latitude. Note difference in vertical scales for the shelf and slope water properties.

Additionally, compared with the interannual anomalies, the seasonal variation in the model slope water properties is small (Figures 3b and 3d), and whether or not it is removed from the record has a negligible effect on the analysis (change in $R^2 < 0.01$). Moreover, the deep salinity bias due to NCOM in turn biases the calculated f_{PEW} of the slope water by ~0.05. However, because this analysis addresses interannual anomalies rather than mean fields, this bias will not have a significant impact on our results.

2.3. Wind Stress

Meridional wind stress (τ_y) was used in this analysis to represent the strength of upwelling. Wind stress was derived from MM5/WRF model winds (Mass et al., 2003), which were also used in the atmospheric forcing of the model. The MM5/WRF model winds generally reproduce observed winds well in the study domain, including high correlation with moored sensors (0.66–0.93), little bias in wind direction in summer, and good agreement with model and observed wind magnitude in fall (ratio model/observed wind strength = 0.99 ± 0.13; Tinis et al., 2006). However, the model winds have a 35° clockwise bias in wind direction in fall and the magnitude of summer model winds is higher than observed (ratio model/observed wind strength = 1.56 ± 0.65; Tinis et al., 2006). Local meridional wind stress was calculated from meridional and zonal wind speed at each latitude (44°N–48°N) at 125°W. Remote wind forcing was represented by meridional wind stress at 40°N, 125°W: near the region of maximum forcing of coastal-trapped waves (Battisti & Hickey, 1984). Meridional wind stress was calculated from 3 hourly meridional and zonal wind speeds, and the resulting stresses were averaged to daily values. Then the same 30 day Hanning filter used with Cascadia model output was applied to the wind stress data to derive monthly values. As above, the mean seasonal cycle was removed from the time series to obtain interannual anomalies.

2.4. Lagrangian Analysis

Within the Cascadia model run, 3 million particles were released at 38 points along the model boundaries (see Figure 1) at every tenth of the full water column depth, once daily from January 2002 to November 2008. For the purpose of this study, we only used particles that were released in the top 600 m of the water column. To avoid double counting, particles that exited the domain within the first 3 days of their release

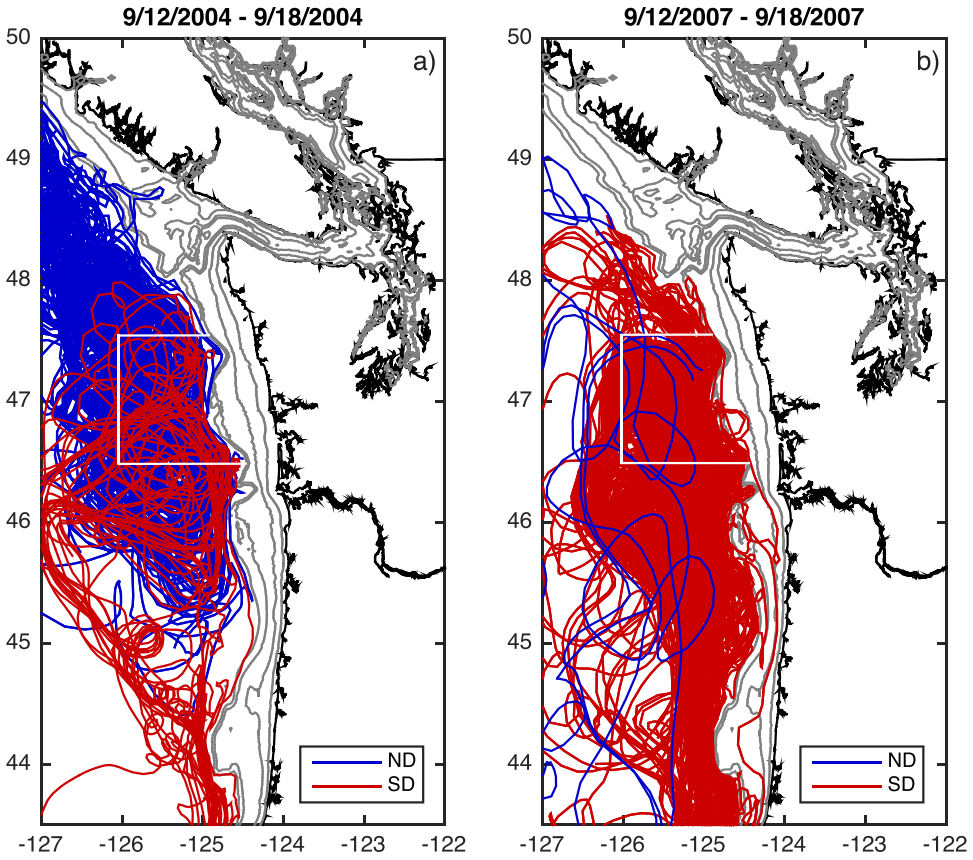

Figure 4. Tracks of Deep particles (released below 150 m depth) that were found on the slope at 47°N (between 46.5°N and 47.5°N; 126°W to the 150 m depth; white box) during 1 week (a) in mid-September 2004 and (b) in mid-September 2007. Particle tracks are colored by source: ND, Northern Deep water (blue); SD, Southern Deep water (red). Release locations of particles are indicated in Figure 1.

were excluded, as well as particles that were released when flow at the model boundary was outward. After application of these criteria, about 203,500 particles remained for use in this analysis, an average of 70 particles per day. Each particle's position in latitude, longitude, and depth was tracked each day until it moved outside the model boundaries or was "beached" on land, defined as being close enough to land that a bilinear interpolation of the ROMS land mask (1 for ocean, 0 for land) at its location was less than 0.5 (Banas et al., 2015). Based on these criteria, average particle lifetime was 61 $\pm$ 78 days. Vertical motion includes a random-displacement scheme for vertical diffusion (Banas et al., 2009; Visser, 1997).

Analysis included particles that were found on the shelf or over the slope at any time during the 2003–2008 record. In this context, the shelf was defined as the bottom half of the water column over the region between 40 and 80 m isobaths. We included the bottom half of the column, rather than just the bottom 1/8 of the water column as was used in the Eulerian analysis, to ensure that there would be enough particles to produce statistically significant results. The slope was defined as the water column between 150 and 500 m over the region between the 150 m isobath and 1° longitude from the 150 m isobath (ranging from 125.5°W to 126.5°W, depending on latitude; Figure 1). The shelf and slope were divided into 1° latitude bands for analysis centered on the sections in the previous analysis, e.g., with 44°N represented by the region between 43.5°N and 44.5°N. On average, there were 42 $\pm$ 19 particles in each 1° shelf band and 1,783 $\pm$ 550 particles in each 1° slope band at each time step. Once any particle moved into the Salish Sea (eastward of 124°W in the Strait of Juan de Fuca; see Figure 1), it was eliminated from analysis. Analysis of these "Salish Sea" particles showed that inclusion of outflow from the Salish Sea results in more particles of deep origin ($\sim$14% more) on the shelf near the Strait of Juan de Fuca (48°N); however, they have very little ($<$1%) influence on water origin in the rest of the domain. All particles were then divided into categories based on where they entered the model domain. These categories are "Southern" (at 43°N, between the

coast and 125.5°W: Figure 1), "Northern" (at 127°W, between 48.5°N and 50°N: Figure 1), and "Offshore" (everywhere else on the model boundary: Figure 1). The Northern and Southern particles were also divided into "Shallow" particles (entering above 150 m depth) and "Deep" particles (entering below 150 m depth). Figure 4 depicts an example of deep particle tracks colored by water origin for particles that end up within the slope box at 47°N for 12–18 September 2004 and 2007.

From here, the fraction of particles (f) from each origin in each region was calculated at every time step (daily). These daily values were integrated over 30 day periods. The seasonal cycle and interannual anomalies for the particle origin fractions in each region were calculated as described above in the Eulerian analysis. Note that the particle release, originally performed for a different application, does not include 2009 and therefore comparisons between the gridded and Lagrangian analyses only span 2003–2008.

As mentioned previously, the entire bottom half of the water column rather than the bottom 1/8 of the water column was included over the shelf to ensure that there were enough particles at each time step to generate statistically significant results. However, due to the dynamics of flow over the shelf, the bottom half of the water column includes both the bottom boundary layer (offshore flow developing later in the upwelling season) and a portion of the interior flow (onshore flow developing over the upwelling season), rather than only the bottom boundary layer as in the Eulerian analysis of shelf water. While the alongshelf flow dominates the cross-shelf flow, this definition leads to a bias in the fraction of "Southern" particles (f_s) of about 20% in the bottom half compared to the bottom 1/8 of the water column. Over the entire record, on average, the f_s of the bottom half of the water column was 0.43 while the f_s of the bottom 1/8 of the water column was 0.52. The effect of this bias on our results is reduced by removal of the mean seasonal cycle when calculating interannual anomalies, and its effect on the R^2 of correlations found in this study is <0.05 in all cases.

3. Results

3.1. Eulerian Analysis

3.1.1. Shelf Water

As expected for any Eastern Boundary Current System, the shelf (bottom 1/8 of the water column between 40 and 80 m isobaths) water experienced a seasonal cycle in its water properties. During the upwelling season, salinity (S_{shelf}) was at its highest, with a mean seasonal high of 33.57 psu (Figure 3a), and temperature (θ_{shelf}) was at its lowest, with a mean seasonal low of 6.99°C (Figure 3c). The standard deviation of the seasonal variation for S_{shelf} was 0.32 psu and 0.83°C for θ_{shelf}. The interannual anomalies in salinity (S'_{shelf}) and temperature (θ'_{shelf}) in shelf water had standard deviations $\sim$0.8 of their seasonal variation (Figure 5). Additionally, there was little difference across latitudes in either salinity or temperature anomalies. Hickey et al. (2016) also found similar anomalies in near-bottom shelf water both seasonally and interannually across a similar latitudinal range using observational data. However, the interannual anomalies observed by Hickey et al. (2016) differed significantly between the summer and winter over their observed time period, with very little variability among summer months and high variability in winter months. This pattern was also evident in the model (Figure 5), with standard deviations during winter months nearly twice those during summer months. All variable symbols and their definitions are outlined in Table 1.

In general, the anomalies in shelf salinity and temperature were inversely correlated ($R^2 = 0.72 \pm 0.05$), i.e., with cold and salty conditions coinciding (Figure 6a). (All correlations mentioned in this paper are significant at the 95% confidence level, with the degrees of freedom (df) calculated using the autocorrelation method, and all significant cross-correlations among variables are outlined in Table 2.) The delayed upwelling in 2005, described by Hickey et al. (2006) and Pierce et al. (2006), is apparent in the transition from negative to positive salinity anomalies and from positive to negative temperature anomalies in late May 2005 (Figure 5). In addition, the unusually warmer and fresher water found on the NCCS shelf in July through October 2004 (Figure 5) was also observed in moored array data at several sites by Hickey et al. (2016).

3.1.2. Slope Water

As expected, the slope ($\sigma_t = 26.25$–27.0 kg m^{-3} isopycnals, between 150 m isobath and 1° longitude offshore of the 150 m isobath) water properties did not show as pronounced a seasonal cycle as did the water on the shelf (Figures 3b and 3d). The standard deviation of interannual anomalies in slope salinity (S'_{slope}), temperature (θ'_{slope}), and fraction of PEW (f'_{PEW}) were about 1.6 times as large as the standard deviation in

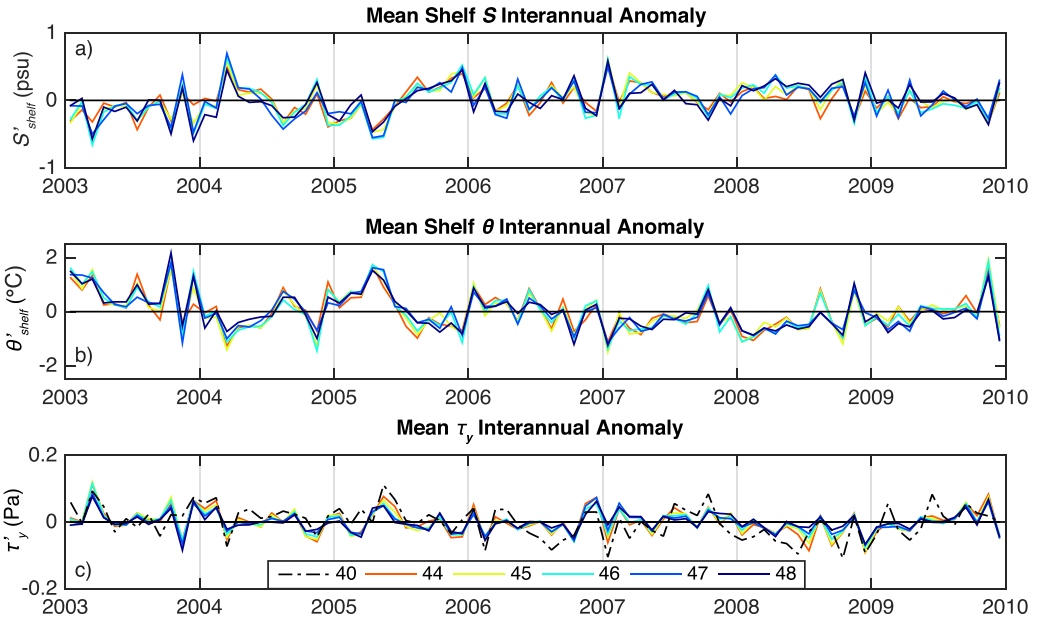

Figure 5. Time series of interannual anomalies in modeled shelf water properties: (a) salinity (S'_{shelf}; psu) and (b) potential temperature (θ'_{shelf}; °C), and (c) meridional wind stress (τ'_y; Pa). Color denotes latitude, with remote wind stress at 40°N plotted in dashed black in Figure 5c. Ticks mark the beginning of each year.

their seasonal variation (Figure 7). Over the record, the mean f'_{PEW} over all latitudes is about 0.31, which is about 0.05 less than observations by Thomson and Krassovski (2010). This difference can be attributed to the salinity bias in the model, as described in section 2.2. Both slope salinity (S_{slope}) and temperature (θ_{slope}) decreased in the summer, as well as with latitude, with a greater seasonal decrease in temperature (Figures 3b and 3d), and S'_{slope} and θ'_{slope} are significantly correlated ($R^2 = 0.30 \pm 0.07$; not significant at 45°N or 48°N; Figure 6b). Thus, cold and fresh conditions generally coincide on the slope, indicative of advection or

Table 1
Definitions of All Analyzed Eulerian and Lagrangian Variables[a]

Variable symbol	Description
Eulerian	
τ_y^{local}	Meridional local wind stress: measured at each latitude (44°N–48°N), 125°W (Pa)
τ_y^{remote}	Meridional remote wind stress: measured at 40°N, 125°W (Pa)
$z_{26.5}$	Depth of the $\sigma_t = 26.5$ kg m^{-3} isopycnal (m)
f_{PEW}	Fraction of Pacific Equatorial Water (PEW)
S_{shelf}	Salinity (psu) on the shelf (bottom 1/8 of the water column between 40 and 80 m isobaths)
θ_{shelf}	Potential temperature (°C) on the shelf (bottom 1/8 of the water column between 40 and 80 m isobaths)
S_{slope}	Salinity (psu) on the slope ($\sigma_t = 26.25$–27.0 kg m^{-3} isopycnals, between 150 m isobath and 1° longitude offshore of the 150 m isobath)
θ_{slope}	Potential temperature (°C) on the slope ($\sigma_t = 26.25$–27.0 kg m^{-3} isopycnals, between 150 m isobath and 1° longitude offshore of the 150 m isobath)
Lagrangian	
f_S^{shelf}	Fraction of southern water (released at 43°N, between coast and 125.5°W) on the shelf (bottom half of the water column between 40 and 80 m isobaths)
f_{Sh}^{shelf}	Fraction of shallow water (released above 150 m depth) on the shelf (bottom half of the water column between 40 and 80 m isobaths)
f_S^{slope}	Fraction of southern water (released at 43°N, between coast and 125.5°W) on the slope (150–500 m depth, between 150 m isobath and 1° longitude offshore of the 150 m isobath)
f_{Sh}^{slope}	Fraction of shallow water (released above 150 m depth) on the slope (150–500 m depth, between 150 m isobath and 1° longitude offshore of the 150 m isobath)

[a]In text, anomalies are indicated by ′.

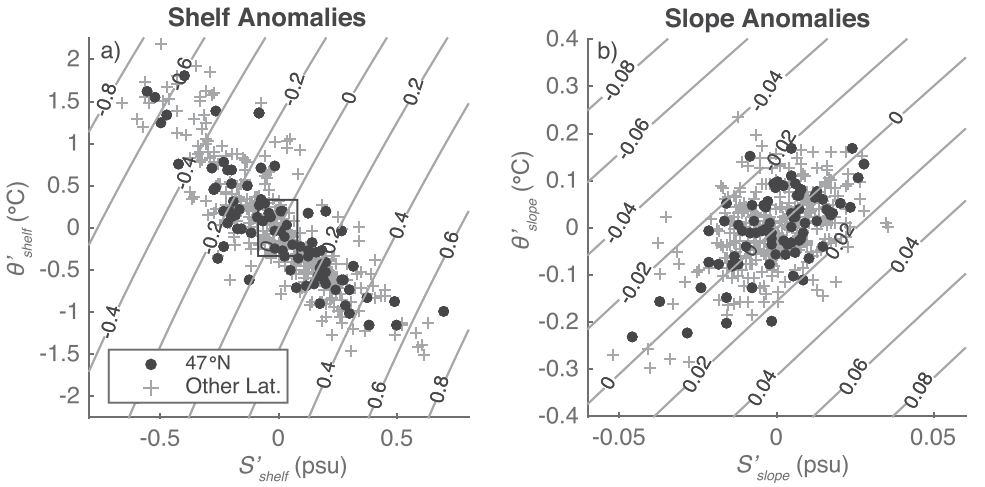

Figure 6. Interannual anomalies in shelf salinity (S'_{shelf}; psu) plotted against interannual anomalies in shelf temperature (θ'_{shelf}; °C; a; $R^2 = 0.72 \pm 0.05$, degrees of freedom (df) = 66.8), and interannual anomalies in slope salinity (S'_{slope}; psu) plotted against interannual anomalies in slope temperature (θ'_{slope}; °C; b; $R^2 = 0.30 \pm 0.07$, df = 23.2; not significant at 45°N or 48°N). Circles denote values at 47°N, + denote all other latitudes, and the isopycnals (anomalies from the record mean shelf and slope density) are plotted in grey. R^2 and df are the mean for all data at 95% confidence. The box on the shelf anomalies plot depicts the range of the slope anomalies within the range of the shelf anomalies.

change along isopycnals, in contrast to the shelf where cold and salty conditions coincide, indicative of advection or change across isopycnals, as mentioned above (Figure 6). Note that the scale of these anomalies on the shelf is an order of magnitude larger than on the slope, and the anomalies in slope water properties are contained within the scatter in anomalies of shelf water (small box embedded in Figure 6a).

Table 2
Significant Cross-Correlations of Interannual Anomalies in All Analyzed Variables

	τ'^{local}_y	τ'^{remote}_y	$z'_{26.5}$	f'_{PEW}	S'_{shelf}	θ'_{shelf}	S'_{slope}	θ'_{slope}	f'^{shelf}_S	f'^{shelf}_{Sh}	f'^{slope}_S	f'^{slope}_{Sh}
τ'^{local}_y												
τ'^{remote}_y	0.37											
$z'_{26.5}$												
f'_{PEW}			*0.21*[a]									
S'_{shelf}	0.44	0.34	*0.18*[b]									
θ'_{shelf}	0.35	0.25	*0.22*[c]	*0.11*[d]	0.72							
S'_{slope}				0.59								
θ'_{slope}			*0.36*[d]	0.83		0.16	*0.30*[e]					
f'^{shelf}_S												
f'^{shelf}_{Sh}									*0.19*[f]			
f'^{slope}_S									*0.43*[e]			
f'^{slope}_{Sh}									*0.21*[g]	*0.10*[h]	*0.36*[h]	

Note. Local wind stress (τ'^{local}_y), remote wind stress (τ'^{remote}_y), depth of the 26.5 kg m^{-3} isopycnal ($z'_{26.5}$), fraction of PEW (f'_{PEW}), shelf salinity (S'_{shelf}), shelf temperature (θ'_{shelf}), slope salinity (S'_{slope}), slope temperature (θ'_{slope}), fraction of southern source water on the shelf (f'^{shelf}_S), fraction of shallow source water on the shelf (f'^{shelf}_{Sh}), fraction of southern water on the slope (f'^{slope}_S), and fraction of shallow water on the slope (f'^{slope}_{Sh}). Correlations are significant at the 95% confidence interval and apply to all latitudes unless otherwise indicated.

[a]Significant at 95% confidence interval for 45°N, 46°N, and 48°N.
[b]Significant at 95% confidence interval for 44°N, 45°N, and 48°N.
[c]Significant at 95% confidence interval for 44°N–46°N, and 48°N.
[d]Significant at 95% confidence interval for 45°N–48°N.
[e]Significant at 95% confidence interval for 44°N, 46°N, and 47°N.
[f]Significant at 95% confidence interval for 44°N and 45°N.
[g]Significant at 95% confidence interval for 46°N–48°N.
[h]Significant at 95% confidence interval for 45°N, 46°N, and 48°N.

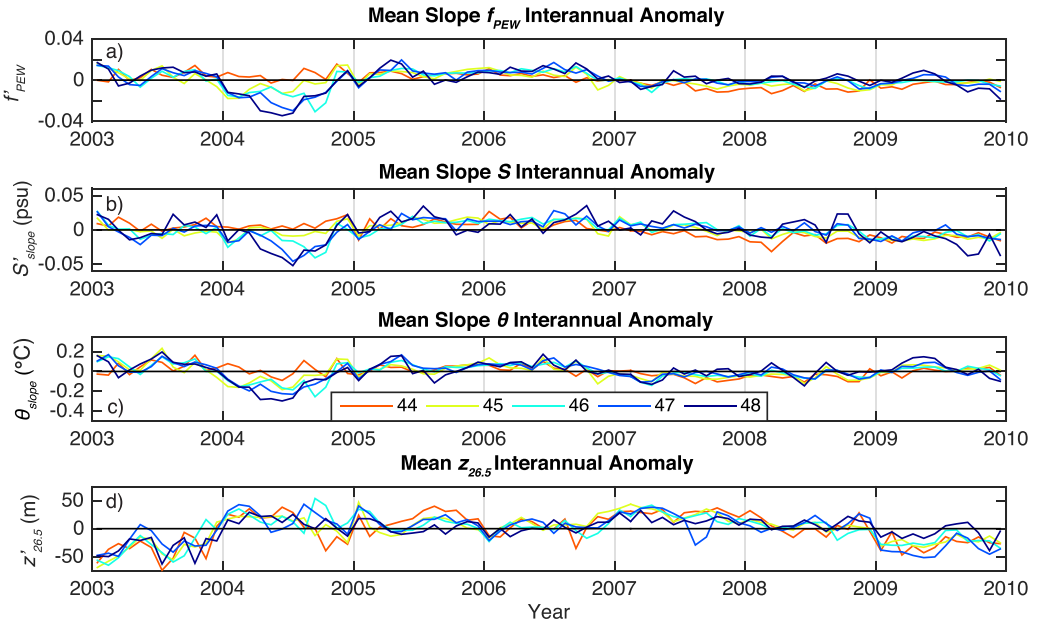

Figure 7. Time series of interannual anomalies in modeled slope water properties: (a) Pacific Equatorial Water (PEW) fraction (f'_{PEW}), (b) salinity (S'_{slope}; psu), (c) potential temperature (θ'_{slope}; °C), and (d) z-position of $\sigma_t = 26.5$ kg m^{-3} isopycnal ($z'_{26.5}$; m), representative of CUC core depth. Color denotes latitude. Ticks mark the beginning of each year.

Throughout most of the time series, S'_{slope}, θ'_{slope}, and f'_{PEW} vary similarly at all latitudes. However, in 2004, there is an unusual poleward gradient in water properties over the slope, with anomalously cold, fresh, and low f_{PEW} in the north (Figure 7). This cold, fresh, and low f_{PEW} water could be indicative of an intrusion of subarctic water from the north (e.g., Kosro, 2003) and could explain the poleward gradient in water properties over the slope. Lagrangian analysis corroborates this interpretation, indicating an anomalously high fraction of water from the north over the slope during the late upwelling season in 2004 (Figure 4; section 3.2).

The 26.5 kg m^{-3} isopycnal represents the core of the CUC (Thomson & Krassovski, 2010); thus $z_{26.5}$ represents the z-position of the CUC and suggests the vertical movement of the CUC in the water column. Seasonally, $z_{26.5}$ varied by about 26 m, with a shoaling of $z_{26.5}$ during the upwelling season (not shown). The mean $z_{26.5}$ over all latitudes ranged from -210 to -184 m over the seasonal cycle. However, the standard deviation in interannual anomalies in the depth of the 26.5 kg m^{-3} isopycnal ($z'_{26.5}$) was about three times as large as the standard deviation of its seasonal variation.

3.1.3. Relationships Between Water Properties and Wind Stress

Interannual anomalies in shelf salinity (S'_{shelf}) were significantly correlated with interannual anomalies in local wind stress ($\tau_y'^{local}$; Figure 8a and Table 2) and remote (40°N) wind stress ($\tau_y'^{remote}$; Figure 8b and Table 2). The correlations suggest that, over all latitudes, on average, local wind variability accounted for about 44 ± 10% of shelf salinity variability, while remote wind variability accounted for about 34 ± 9% of shelf salinity variability (Table 2). August values are displayed in these figures to highlight the upwelling season, although the local and remote wind stress correlations include the entire year.

Likewise, interannual anomalies in shelf salinity (S'_{shelf}) were significantly correlated with interannual anomalies in CUC z-position ($z'_{26.5}$; Figure 8c and Table 2). For 44°N, 45°N, and 48°N, variability in $z'_{26.5}$ accounted for 18 ± 5% of S'_{shelf} variability, such that when the CUC is shallower, the shelf water is saltier. Correlations of S'_{shelf} and $z'_{26.5}$ at 46°N and 47°N were not significant (Table 2).

Similar to shelf salinity anomalies, temperature anomalies (θ'_{shelf}) were significantly correlated with $\tau_y'^{local}$ ($R^2 = 0.35 \pm 0.07$; Table 2) and $\tau_y'^{remote}$ ($R^2 = 0.25 \pm 0.04$; Table 2) and with anomalies in $z'_{26.5}$ ($R^2 = 0.22 \pm 0.09$, excluding 47°N; Table 2). Additionally, θ'_{shelf} was weakly, but significantly, correlated with fraction of PEW (f'_{PEW}, $R^2 = 0.11 \pm 0.01$, excluding 47°N; Table 2). As expected, $\tau_y'^{local}$ and $\tau_y'^{remote}$ were significantly correlated, with an average $R^2 = 0.37 \pm 0.11$ (Table 2).

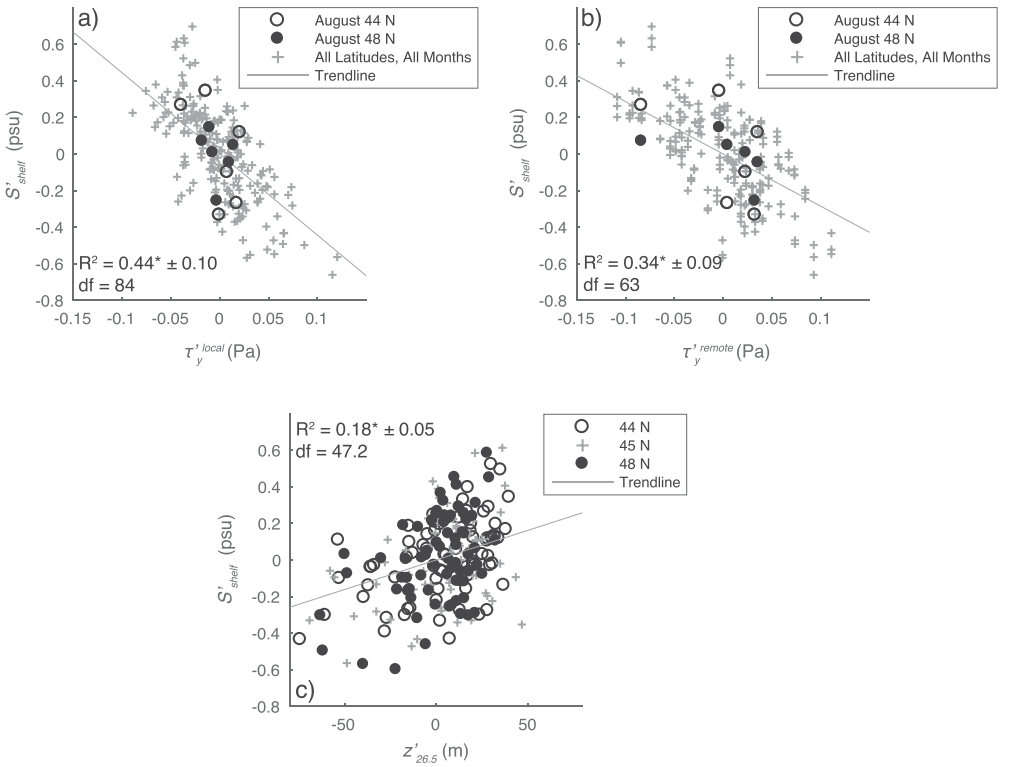

Figure 8. Interannual anomalies in shelf salinity (S'_{shelf}; psu) plotted against (a) interannual anomalies in local wind stress ($\tau_y'^{local}$; Pa), (b) interannual anomalies in remote wind stress ($\tau_y'^{remote}$; Pa), and (c) interannual anomalies in CUC core depth ($z'_{26.5}$; m). For Figures 8a and 8b, open circles denote August values at 44°N, filled circles denotes August values at 48°N, + denote all latitudes during all months of the year, and the trend line is plotted in grey. R^2 and df are the mean for all data at 95% confidence. For Figure 8c, open circles denote values at 44°N, + denote values at 45°N, filled circles denote values 48°N, and the trend line is plotted in grey. R^2 and df are the mean for 44°N, 45°N, and 48°N at 95% confidence.

Slope temperature anomalies (θ'_{slope}) were also significantly correlated with $z'_{26.5}$ ($R^2 = 0.36 \pm 0.09$, excluding 44°N; Table 2) and f'_{PEW} ($R^2 = 0.83 \pm 0.07$; Table 2). Similarly, slope salinity anomalies (S'_{slope}) were correlated with f'_{PEW} ($R^2 = 0.59 \pm 0.11$; Table 2). Also, interannual anomalies in $z'_{26.5}$ and f'_{PEW} were correlated at 45°N, 46°N, and 48°N, with an average $R^2 = 0.21 \pm 0.01$ with a deeper undercurrent carrying a greater PEW fraction (Table 2). No other significant correlations were found among shelf water properties, slope water properties, or wind stress.

To better account for cross-correlation among the three forcing variables discussed above (local wind stress ($\tau_y'^{local}$), remote wind stress ($\tau_y'^{remote}$), and CUC core depth ($z'_{26.5}$)), a Generalized Linear Model (GLM; Nelder & Wedderburn, 1972) was constructed for the interannual shelf salinity anomalies (S'_{shelf}) record at each latitude, based on anomalies in the three forcing variables. The interannual variability in shelf salinity was reasonably well reconstructed by the GLM, with an average $R^2 = 0.58 \pm 0.08$ for all latitudes. The best fit was at 48°N with $R^2 = 0.69$ (Figure 9).

3.2. Lagrangian Analysis

3.2.1. Shelf

The shelf (bottom half of the water column between 40 and 80 m isobaths) experienced high variability in water origin both seasonally (Figures 10a–10e) and interannually (Figures 11a–11e). The standard deviations in interannual anomalies in water origin were about 1.4 times the standard deviations in the seasonal variation. Throughout the entire record, shelf water was mostly composed of shallow water (NSh and SSh, Figures 11a–11e), although there were occasional intrusions of northern deep water (ND, Figures 11a–11e) that are consistent with the timing of deep northern water intrusions on the slope (ND, Figures 11f–11j). At northern latitudes, northern water (ND and NSh, Figures 10a–10e) dominated the water on the shelf during the upwelling season, consistent with the equatorward coastal jet associated with upwelling. At southern

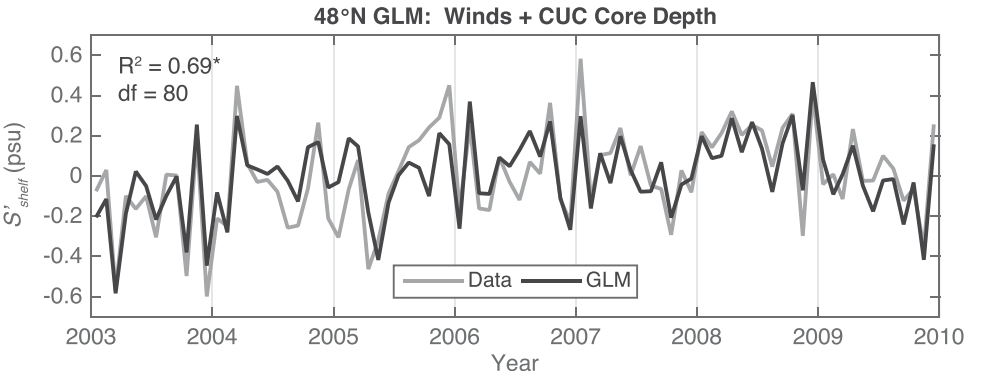

Figure 9. Time series of interannual anomalies in shelf salinity (S'_{shelf}, psu) at 48°N (gray) plotted with time series of GLM of interannual anomalies in shelf salinity (S'_{shelf}, psu) at 48°N (black), recreated using interannual anomalies in local wind stress ($\tau_y'^{local}$; Pa), remote wind stress ($\tau_y'^{remote}$; Pa), and CUC core depth ($z'_{26.5}$; m). R^2 =0.69 (significant at 95% confidence), degrees of freedom = 80.

latitudes, southern water (SD and SSh, Figures 10a–10e) dominated the water on the shelf, with a small increase in northern water during the upwelling season. There are also small amounts of southern deep water present on the shelf during the late summer into fall (SD, Figures 10a–10e), and this pattern is more evident in some years, like 2005, than in others, like 2004 (SD, Figures 11a–11e). During the winter shelf water transitioned to mostly southern water (SD and SSh, Figures 10a–10e), consistent with the poleward flow associated with downwelling, as well as the larger-scale Davidson Current.

3.2.2. Slope

On the slope (150–500 m depth; between 150 m isobath and 1° longitude offshore of 150 m isobath), water origin varied more interannually (Figures 11f–11j) than it did seasonally (Figures 10f–11j). The standard

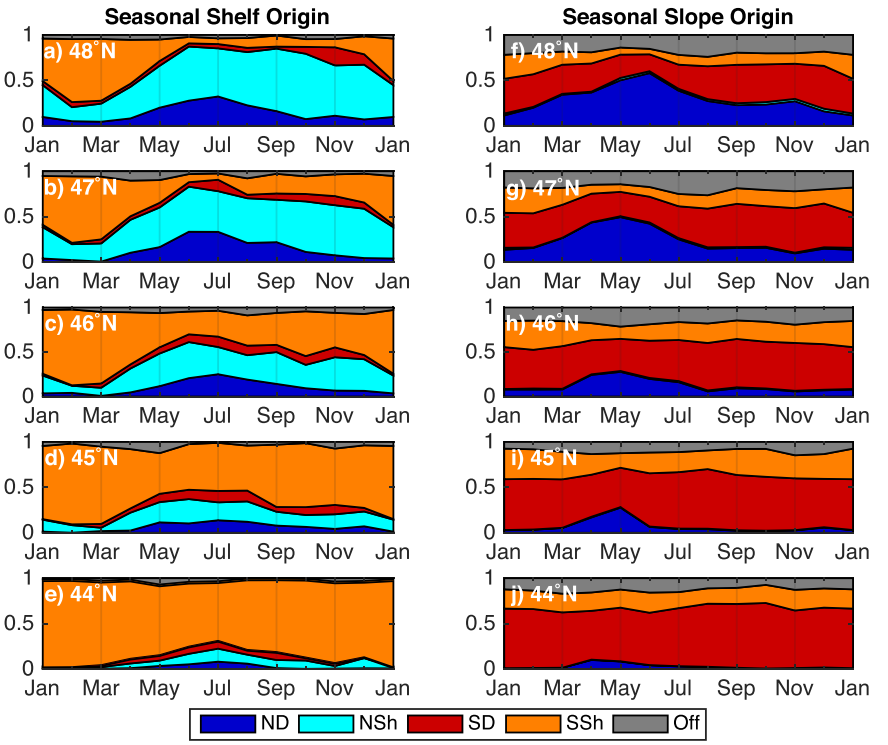

Figure 10. Seasonal fraction (a–e) of shelf water and (f–j) of slope water for each latitude (44°N–48°N) colored by origin. ND, Northern Deep water (blue); NSh, Northern Shallow water (cyan); SD, Southern Deep water (red); SSh, Southern Shallow water (orange); and Off, Offshore water (grey). Deep and shallow releases were divided by the 150 m depth contour. Release locations of particles are indicated in Figure 1. Ticks mark the beginning of each month.

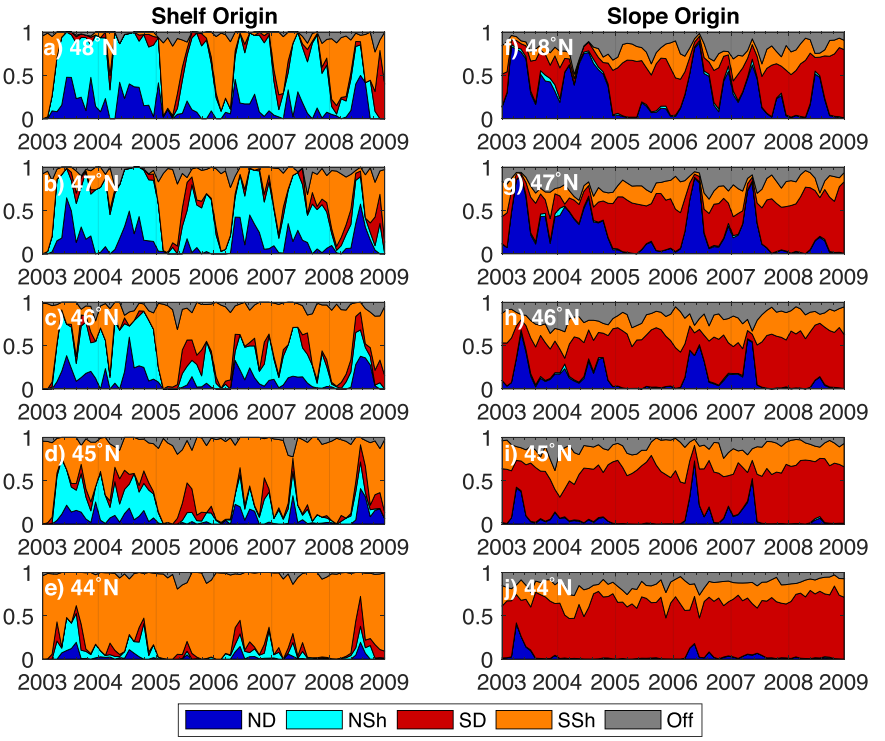

Figure 11. Full monthly averaged time series of fraction of (a–e) shelf water and (f–j) slope water for each latitude (a–e; 44°N–48°N) colored by origin, colors as in Figure10. The seasonal cycle was not removed. Deep and shallow releases were divided by the 150 m depth contour. Release locations of particles are indicated in Figure 1. Ticks mark the beginning of each year.

deviations in interannual anomalies in slope water origin were about 1.8 as large as the standard deviations in their seasonal variation. Throughout the entire record, the slope was mostly composed of deep water (ND and SD) as compared to shallow water (NSh and SSh, Figures 11f–11j). Southern deep water (SD, Figures 10f–10j) increased over the upwelling season, ultimately dominating the water on the slope, while northern deep water increased during the winter into the spring when the CUC is absent (ND, Figures 10f–10j). This seasonal pattern is expected, and suggests the CUC gradually flushing out northern water over the upwelling season as it develops each year. The increase in northern deep water on the slope during winter into spring (ND, Figures 10f–10j) could be indicative of the Washington Undercurrent, a deep equatorward current that sometimes flows over the Washington slope during winter months (Hickey, 1989). The increase in northern water present on the slope with latitude is consistent with hydrographic results from Thomson and Krassovski (2010).

3.2.3. Relationships Between Water Sources

Interannual anomalies in the fraction of southern water (shallow (SSh) and deep (SD) combined) in the slope water ($f'_S{}^{slope}$) and over the shelf ($f'_S{}^{shelf}$) were significantly correlated over most of the model domain (45°N–48°N), with average $R^2 = 0.43 \pm 0.10$, although the correlation at 44°N was not significant (Figure 12 and Table 2). The intrusions of northern water on the slope (Figures 11f–11j) coincided with intrusions of northern water on the shelf (Figures 11a–11e). The strong intrusion of northern deep water of 2004 (ND, Figures 4 and 11f–11j) may have been responsible for the unusual poleward gradient in water properties, with colder, fresher water to the north, over the slope in 2004 (Figure 7). The difference in water origin on the slope in the anomalous 2004 year as compared to a typical year like 2007 is especially apparent in the tracks of particles colored by water origin in Figure 4.

The anomalies in the fraction of southern water (f'_S) represents north and south water masses since the offshore fraction (f'_{Off}) has a smaller interannual variation on both the shelf and slope (standard deviation = 0.05, 0.07, respectively) as compared to the southern fraction (f'_S; standard deviation = 0.20, 0.17, respectively) and northern fraction (f'_N; standard deviation = 0.21, 0.15, respectively) on the shelf and

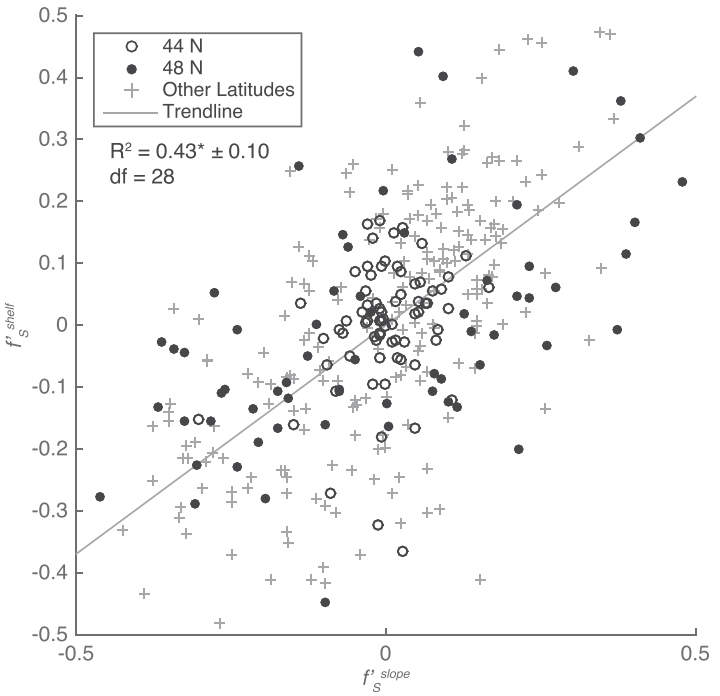

Figure 12. Interannual anomalies in fraction of southern water on the shelf (f'^{shelf}_S) plotted against interannual anomalies in fraction of southern water on the slope (f'^{slope}_S). Open circles denote values at 44°N, filled circles denote values at 48°N, + denote other latitudes, and the trend line is plotted in grey. R^2 and df are for all data excluding 44°N at 95% confidence.

slope. So, any loss in southern water is largely replaced by northern water, as expected. Weaker correlations that were significant within some, but not all, of the model domain between f'_S and anomalies in fraction of shallow water (f'_{Sh}) are outlined in Table 2. The Lagrangian metrics f'_S and f'_{Sh} were not significantly correlated with any variable from the Eulerian analysis discussed previously, for either the slope or the shelf, for a combination of numerical and dynamical reasons, as discussed below.

4. Discussion

4.1. Upwelling System Dynamics

Interannual anomalies in shelf (bottom 1/8 of the water column between 40 and 80 m isobaths) salinity (S'_{shelf}) and temperature (θ'_{shelf}) were significantly correlated with each other ($R^2 = 0.72 \pm 0.05$), with an inverse relationship, aligned approximately orthogonal to isopycnals (Figure 6a). This relationship suggests that variation in the strength, vertical structure, and apparent source depth of upwelling largely drives the relationship between salinity and temperature on the shelf. Slope ($\sigma_t = 26.25$–27.0 kg m^{-3} isopycnals, between 150 m isobath and 1° longitude offshore of the 150 m isobath) water properties, including salinity (S'_{slope}), temperature (θ'_{slope}), and fraction of PEW (f'_{PEW}), did not vary nearly as much as properties on the shelf: the variance in shelf water properties was about 10 times the variance in slope water properties, and variance in slope water properties are contained within the scatter of shelf water properties (Figures 5–7). Additionally, while S'_{slope} and θ'_{slope} were weakly correlated ($R^2 = 0.30 \pm 0.07$; not significant at 45°N or 48°N), they display the opposite relationship, varying from cold, fresh water to warm, salty water (Figure 6b). This relationship suggests that variation in slope water properties is driven by changes in water origin or advection along-isopycnal surfaces, like alongcoast advection or changes in the composition of the CUC. This incompatibility in temperature-salinity relationships between shelf and slope water would explain why neither S'_{slope} nor f'_{PEW} were significantly correlated with S'_{shelf} ($R^2 = 0.04 \pm 0.04$, $R^2 = 0.01 \pm 0.01$, respectively), while θ'_{shelf} and θ'_{slope} were significantly correlated ($R^2 = 0.16 \pm 0.04$; Table 2). Therefore, interannual variability in slope water composition does not appear to be the primary driver of variability in shelf salinity and temperature. This is not necessarily the case for other tracers with different vertical and alongcoast gradients, however, and we consider the implications of these temperature/salinity patterns for dissolved oxygen and dissolved inorganic carbon in section 4.3.

From the results of the Generalized Linear Model recreation of the shelf salinity record, it can be concluded that together, interannual variability in both local and remote alongshore wind stress and in depth of the CUC core account for more than half of the interannual variability in shelf water salinity. Variability in local and remote wind stress represent the variability in the strength and persistence of upwelling, with stronger upwelling leading to saltier shelf water. The vertical position of the CUC in the water column might also reflect variability in the alongshore wind patterns because the CUC is, in part, driven by the gradient in alongshore wind stress. Hickey et al. (2016) highlight 2004, a year with warmer and fresher shelf water and a shallower, warmer, and fresher CUC, and link these anomalies to weaker remote and local winds along the coast and a loss of the alongshore wind stress gradient. Thus, we conclude that variability in shelf water properties is largely caused by variability in local and remote wind stress, both directly and through the wind's role in setting the vertical position of the CUC.

As discussed previously, there is a significant, though weak, correlation between CUC core depth and shelf salinity in most, but not all, of the model domain. This correlation is strongest near the boundaries and weakens in the model interior, with no significant correlation at 46°N and 47°N ($R^2 = 0.08$ and 0.03, respectively). The lack of significant correlation at 46°N and 47°N may be due to local topography, including shelf

break canyons, or other local shelf processes. While canyons in the region, specifically the Quinault Canyon (46°N) and Astoria Canyon (47°N), enhance upwelling to the shelf, the development of the CUC can shut down this enhancement later in the upwelling season, except during periods of wind relaxation (Connolly & Hickey, 2014; Hickey, 1989, 1997), to an extent that we speculate could depend on CUC core depth. This complicated interaction between the CUC and enhanced canyon upwelling, as well as the highly three-dimensional circulation in the region overall, makes it difficult to isolate the exact cause of the reduced correlation.

While anomalies in shelf salinity (S'_{shelf}) are significantly correlated with variability in the depth of the CUC core ($z'_{26.5}$), they are not significantly correlated with anomalies in slope water composition, in particular, fraction of PEW (f'_{PEW}) and salinity (S'_{slope}). This lack of correlation is consistent with the fact, as noted above, that temperature and salinity anomalies have incompatible relationships on the shelf and slope (Figure 6). Consequently, on the interannual timescale, the vertical position of the CUC might matter more to shelf water properties than its composition. However, it is possible that other local processes could be obscuring the direct influence of slope water, a possibility supported by the link between slope and shelf water origin through large-scale advection, as discussed in the next section.

4.2. Large-Scale Alongcoast Advection

The correlation of slope (150–500 m depth; between 150 m isobath and 1° longitude offshore of 150 m isobath) and shelf (bottom half of the water column between 40 and 80 m isobaths) water shows that both are affected by large-scale advection of water through the northern and southern boundaries (f'^{slope}_S and f'^{shelf}_S, $R^2 = 0.43 \pm 0.10$, excluding 44°N; Figure 12). Furthermore, slope and shelf water properties are more strongly linked interannually through large-scale advection processes north and south (f'^{slope}_S and f'^{shelf}_S, $R^2 = 0.43 \pm 0.10$; excluding 44°N; Figure 12) than they are directly linked to each other through their composition (S'_{slope} and S'_{shelf}, $R^2 = 0.04 \pm 0.04$, not significant).

Freeland et al. (2003) measured colder and fresher water between 30 and 150 m depth in summer 2002 along both the Newport Hydrographic Line and Line-P, suggesting an intrusion of subarctic water at depths spanning both the midshelf and part of the upper slope. They attribute this invasion of northern water to a stronger equatorward California Current and weaker poleward Alaska and Davidson Currents during spring 2002, although variability in downwelling and mixing during the winter, as well as enhanced flow of the North Pacific Current, may have also played a role.

At more northern latitudes (47–48°N), northern water is evident in both shelf and slope water, but at the southern end of the domain (44°N), Lagrangian results showed that northern water is more present on the shelf than on the slope (Figure 11). Nevertheless, on the slope, intrusions of northern water can extend south to 45°N so that in some years, the WA slope water is not composed of southern water. For example, there is much more northern deep water present on the slope at 47°N in September 2004 than there was in September 2007, when southern water dominates the region (Figure 4). Similarly, Rivas and Samelson (2011), using a Lagrangian analysis in a different model, found that north of Cape Blanco (~43°N), there is more water of northern origin in the Oregon upwelling zone (water column east of the 200 m isobath) than water of southern origin.

Interannual anomalies in shelf salinity and the fraction of southern water on the shelf were not significantly correlated at the 95% confidence level (S'_{shelf} and f'^{shelf}_S, $R^2 < 0.07$), nor were interannual anomalies in wind stress and fraction of southern water on the shelf or slope (τ'^{local}_y, τ'^{remote}_y, f'^{shelf}_S, and f'^{slope}_S, $R^2 < 0.06$). Somewhat surprisingly, interannual anomalies in fraction of PEW and fraction of southern water over the slope were also not significantly correlated (f'_{PEW} and f'^{slope}_S, $R^2 = 0.11 \pm 0.06$), despite the fact that both statistics attempt to represent the same feature: variations in the California Undercurrent. Changes in f_{PEW} might occur through processes like mixing and eddy shedding since f_{PEW} is calculated from temperature and salinity. When Thomson and Krassovski (2010) mapped the CUC by its PEW signature from Oregon to Alaska, they saw a steady, poleward decrease in f_{PEW} through along-isopycnal mixing. Pierce et al. (2000) describes examples of eddies shedding from the CUC, and Pelland et al. (2013) estimates that this generation of anticyclonic eddies, or "cuddies," accounts for about 44% of heat and salt loss as the CUC moves poleward. However, f^{slope}_S on the slope cannot be altered through these processes due to the methods of particle tracking: when "southern" model particles mix with other water, they are not transformed into "northern" particles. Likewise, if PEW is advected north with the CUC and then re-enters the model domain from the

Table 3
Change in Salinity (S) and Inferred Change in Oxygen (O_2) and Dissolved Inorganic Carbon (DIC) due to Vertical Advection (Δ_z) and Alongcoast Advection (Δ_y)

	Δ_z (stdev)	Δ_y (stdev)	Δ_y (2004 event)[a]
S (psu)	0.23	0.01	0.03
O_2 (μmol kg^{-1})	−28	−6	-16 ± 6
DIC (μmol kg^{-1})	29	9	25 ± 9

Note. Signs reported are for positive change in Δ_z and Δ_y.
[a]Gradient in slope water across affected latitudes (45°N–48°N).

north during a subarctic intrusion, the Lagrangian analysis would not count this PEW as "southern" in the calculation of f_S.

4.3. Applications to Biology and Chemistry

As seen in the GLM analysis, variability in local and remote wind stress and in CUC depth contribute to anomalies in the density of water over the shelf. These processes are all part of upwelling variability, which includes strength, vertical structure, and apparent source depth of upwelling, and may lead to changes in shelf water chemistry. The mean change in upwelling variability and its subsequent effects on salinity, oxygen, and dissolved inorganic carbon (DIC) concentrations are summarized in Table 3. We denote anomalies associated with upwelling variability, or across-isopycnal or vertical variation, with a subscript z, in contrast to anomalies associated with alongcoast variations (subscript y). Because the variation in shelf salinity is almost entirely across-isopycnal, ΔS_z is approximately equal to the magnitude of standard deviation of shelf salinity ($\Delta S_z = 0.23$ psu; Table 3). The scale of variation in shelf oxygen (ΔO_z) associated with across-isopycnal salinity/temperature variation can be estimated as follows:

$$\Delta O_z = \frac{\partial O}{\partial z}\,\Delta z$$

where $\partial O/\partial z$ is the gradient of oxygen with depth and Δz is the variation in depth of upwelling source water reflected in ΔS_z. Rewriting in terms of the vertical salinity gradient $\partial S/\partial z$,

$$\Delta O_z = \frac{\partial O}{\partial z}\left(-\frac{\partial S}{\partial z}\right)^{-1}\Delta S_z$$

Using mean dissolved oxygen profiles along the Newport Hydrographic Line (44.65°N) in Pierce et al. (2012) and salinity profiles from the model, $\Delta O_z \approx -28$ μmol kg^{-1}, with a decrease in oxygen concentration with stronger upwelling, which might include deeper apparent depth of upwelled water, stronger upwelling-favorable winds, or shoaling CUC (Table 3). This value is comparable to observed and modeled interannual anomalies in dissolved oxygen on the Washington shelf (Connolly et al., 2010; Siedlecki et al., 2015).

Likewise, the scale of anomalies in DIC associated with observed anomalies in shelf salinity can be estimated as

$$\Delta DIC_z = \frac{\partial DIC}{\partial z}\left(-\frac{\partial S}{\partial z}\right)^{-1}\Delta S_z$$

Combining mean profiles of DIC along the Newport Hydrographic Line (44.65°N) from Feely and Sabine (2011) with model salinity, $\Delta DIC_z \approx 29$ μmol kg^{-1}, with an increase in DIC concentration with stronger upwelling (Table 3). These results suggest that depending on the vertical structure of the water column, stronger upwelling could raise the hypoxic boundary (DO < 60 μmol kg^{-1}) and the aragonite saturation horizon ($\Omega_{arag} < 1$) higher in the water column than is tolerable for native organisms.

Interannual variability in the north-south source of water over the slope and shelf may also translate into changes in chemistry. Scales of variation in alongcoast lateral advection and its subsequent effects on salinity, oxygen, and DIC concentrations are estimated in Table 3. Because the variation in slope salinity is contained within the scatter of the shelf salinity, we estimate ΔS_y on the shelf as the standard deviation of slope salinity ($\Delta S_y = 0.01$ psu; compare Figures 6a and 6b). By analogy with the ΔO_z calculation above,

$$\Delta O_y = \frac{\partial O}{\partial y}\left(-\frac{\partial f_{PEW}}{\partial y}\right)^{-1}\Delta f_{PEW_y}$$

where $\partial O/\partial y$ and $\partial f_{PEW}/\partial y$ are the gradients in oxygen and f_{PEW} with latitude and Δf_{PEW} is the scale of variation in f_{PEW} observed in the model. Using mean oxygen fields along the $\sigma_t = 26.5$ kg m^{-3} isopycnal from the World Ocean Atlas (Garcia et al., 2014), we find that $\Delta O_y \approx -6$ μmol kg^{-1}, with southern water carrying less dissolved oxygen than northern water (Table 3). This value represents the expected variation in oxygen

concentrations in upwelling source water associated with the alongcoast advection anomalies observed in the model analysis.

Accordingly, on average over the time series, the expected variation in oxygen due to along-isopycnal advection (ΔO_y) is small compared to that due to upwelling variability (ΔO_z), but this is not necessarily the case for individual events. The northern intrusion event in 2004, evident in negative f_{PEW} anomalies from 45°N to 48°N (Figure 7), corresponded to an increase in dissolved oxygen of about 16 ± 6 μmol kg^{-1}, as well as decrease in salinity by about 0.03 psu (Table 3). This change in oxygen is similar to the interannual variations in source water oxygen concentration (12 μmol kg^{-1}) observed at Newport, Oregon by Peterson et al. (2013), and is comparable to the effect (ΔO_z) of weaker upwelling, such as shoaling of apparent source depth of upwelled water or deepening of the CUC by 50 m. Note that the effect of the 2004 intrusion event on salinity is still quite small compared to the typical ΔS_z (Table 3).

Similarly, the scale of anomalies in DIC associated with alongcoast lateral advection can be estimated as

$$\Delta DIC_y = \frac{\partial DIC}{\partial y}\left(-\frac{\partial f_{PEW}}{\partial y}\right)^{-1}\Delta f_{PEW\,y}$$

Using mean DIC fields along the $\sigma_t = 26.5$ kg m^{-3} isopycnal from Feely and Sabine (2011), we find that $\Delta DIC_y \approx 9$ μmol kg^{-1}, with southern water carrying more DIC than northern water (Table 3). Like ΔO_y, on average ΔDIC_y is smaller than ΔDIC_z, but individual events can yield ΔDIC_y of similar scale as ΔDIC_z. In the case of the 2004 intrusion of northern water, the negative f_{PEW} anomalies from 45°N to 48°N (Figure 7) corresponded to a decrease in DIC by about 25 ± 9 μmol kg^{-1} (Table 3).

Thus, while on average, ΔO_z and ΔDIC_z are greater than ΔO_y and ΔDIC_y, large-scale intrusion events, such as the northern intrusion event in 2004, can yield ΔO_y and ΔDIC_y of similar scale as mean ΔO_z and ΔDIC_z. Furthermore, the scale of ΔO_y of these intrusion events is of similar size as interannual variation in source water oxygen concentrations described in Peterson et al. (2013). The interannual anomalies in oxygen in Peterson et al. (2013) were statistically linked to changes in NPGO, with positive oxygen anomalies in years with positive NPGO values. The NPGO is driven by changes in the North Pacific Current, with more northern water transported into the region in positive NPGO years. This mechanism is consistent with the idea that there is more oxygen present in the NCCS when there is more northern water advected into the region (Table 3). Overall, the model supports the statistical relationship found by Peterson et al. (2013) and provides a model-based map of what changes in advection by the NPGO might look like.

While the length of the time series from the model prohibits systematic comparison with indices of climate-ocean decadal variability, the mechanisms described in this analysis, particularly changes in the depth of the CUC and alongshore advection, are likely important mechanistic links between climate-ocean decadal modes and the shelf. With the positive phase of the Pacific Decadal Oscillation (PDO; Chhak & Di Lorenzo, 2007), North Pacific Gyre Oscillation (NPGO; Di Lorenzo et al., 2008), and El Nino-Southern Oscillation (ENSO; Jacox et al., 2015; Schwing et al., 2002), the depth of source water to the shelf is shallower, and thus (we might expect in general) poorer in nutrients and oxygen. With the negative phase of each of these indices, the opposite is true. With PDO (Keister et al., 2011) and ENSO (Kosro, 2002), the positive phase of each would lead to more southern source water in the region, with El Nino leading to enhanced poleward flow over the slope and shelf, as observed in Huyer and Smith (1985). However, with NPGO, the positive phase leads to more northern source water in the region, as well as more oxygen (Peterson et al., 2013). Therefore, with respect to nutrients and oxygen, the vertical and alongshore effects of the NPGO reinforce each other, while with both PDO and ENSO the effects on source water depth and advection are likely to counteract each other. The reinforcement of these effects by the NPGO is likely the reason for the statistical link between oxygen concentrations and NPGO, but not oxygen and PDO, described by Peterson et al. (2013). Longer model or observational time series are required to test this conceptual picture.

5. Conclusions

Using an ROMS hindcast model spanning 2003–2009, as well as intensive particle tracking, we studied the interannual variability of shelf water properties with the goal of understanding how the composition and

depth of the California Undercurrent, alongcoast advection, as well as local and remote wind stress, influence this variability. The main conclusions for this analysis are:

1. *Alongcoast interannual variability in both midshelf bottom water and upper slope water properties vary little across 800 km of latitude.*

   Over the whole study domain, there is very little variance between latitudes in temperature and salinity of shelf water, with standard deviation across latitudes in temperature of 0.70 ± 0.04°C, and in salinity of 0.23 ± 0.02 psu (Figure 5), with more variance in winter than in summer. This result is consistent with the results of Hickey et al. (2016) based on data from sensors moored midshelf across a similar range of latitudes. Similarly, temperature, salinity, fraction of PEW, and depth of the 26.5 kg m^{-3} isopycnal on the slope also experienced very little variance in their interannual anomalies between latitudes, with average standard deviation across latitudes in temperature of 0.08 ± 0.02°C, in salinity of 0.01 ± 0.003 psu, in fraction of PEW of 0.01 ± 0.002, and in depth of the 26.5 kg m^{-3} isopycnal of 24 ± 3 m (Figure 7). There is an exception to this pattern on slope in 2004. Lagrangian analysis on the slope suggests that the poleward gradient of cold, fresh water on the slope was due to an intrusion of northern water (Figures 4 and 11f–11j).
2. *Together, interannual variability in local and remote wind stress and in depth of the CUC explain more than half of the interannual variability in midshelf bottom water salinity.*

   Interannual anomalies in local wind stress and in remote wind stress are significantly correlated with interannual anomalies in shelf salinity, with stronger wind stress leading to saltier shelf water ($\tau_y'^{local}$ and S'_{shelf}, $R^2 = 0.44 \pm 0.10$; Figure 8a; $\tau_y'^{remote}$ and S'_{shelf}, $R^2 = 0.34 \pm 0.09$; Figure 8b). Interannual anomalies shelf salinity was also correlated with interannual anomalies in the depth of the 26.5 kg m^{-3} isopycnal ($z'_{26.5}$ and S'_{shelf}, $R^2 = 0.18 \pm 0.05$ for 44°N, 45°N, and 48°N; Figure 8c). To account for cross-correlation among the local and remote wind stress, and in depth of the 26.5 kg m^{-3} isopycnal, a generalized linear model (GLM) was constructed using the interannual anomalies in these three variables to reproduce interannual anomalies in shelf salinity. The resulting GLM suggests that together, interannual anomalies in local and remote wind stress and in depth of the 26.5 kg m^{-3} isopycnal account for more than half the variability in shelf salinity (Generalized Linear Model mean over all latitudes: $R^2 = 0.58 \pm 0.08$). The best fit for this GLM was at 48°N (Figure 9).
3. *The midshelf bottom and upper slope have incompatible relationships between temperature and salinity anomalies*.

   Interannual anomalies in salinity and temperature on the shelf are significantly correlated with an inverse relationship (S'_{shelf} and θ'_{shelf}, $R^2 = 0.72 \pm 0.05$; Figure 6a), while on the slope, salinity and temperature interannual anomalies are significantly correlated with a direct relationship (S'_{slope} and θ'_{slope}, $R^2 = 0.30 \pm 0.07$ for 44°N, 46°N, and 47°N; Figure 6b). Furthermore, the magnitude of variation in slope water properties is about one tenth that of shelf water properties, with the scale of slope variation (Figure 6b) fitting into the scatter around the primary axis of variation on the shelf (Figure 6a). The relationship on the shelf suggests cross-isopycnal variation associated with upwelling dynamics, while the relationship on the slope suggests along-isopycnal variation in water origin.
4. *The vertical position of the CUC might affect shelf water properties more than variations in its composition on the interannual timescale.*

   As discussed above, the patterns of temperature and salinity on the shelf and slope have opposite relationships. Furthermore, changes in CUC properties appear to have a minor effect on shelf water properties (f'_{PEW}, S'_{slope}, and S'_{shelf}, $R^2 = 0.03 \pm 0.03$), as compared with the vertical position of the CUC ($z'_{26.5}$ and S'_{shelf}, $R^2 = 0.18 \pm 0.05$ for 44°N, 45°N, and 48°N; Figure 8c).
5. *The origins of both midshelf bottom water and upper slope water are affected by large-scale alongcoast advection.*

   Lagrangian analysis of origin of shelf and slope water show that both are affected by large-scale alongcoast advection of water from the north and south ($f_S'^{slope}$ and $f_S'^{shelf}$, $R^2 = 0.43 \pm 0.10$, excluding 44°N; Figure 12). Intrusions of northern water are evident on both the shelf and slope, and the frequency of these intrusions varies interannually. These changes in water origin can be indicative of the characteristics of that water, with warm, salty water carried from the south and cold, fresh water carried from the north. In particular, the poleward gradient in cold, fresh water over the slope in 2004 found in the

Eulerian analysis (Figure 7) coincides with an intrusion of northern water in the Lagrangian analysis (Figures 4 and 11f–11j).

6. *Particularly large northern or southern intrusion events can cause changes in shelf water chemistry of the same magnitude as those caused by typical upwelling variability.*

On average, changes in oxygen concentration (-28 μmol kg^{-1}) and in dissolved inorganic carbon concentration (29 μmol kg^{-1}) through upwelling variability (i.e., variability in strength, vertical structure, and apparent source depth of upwelling) are larger than changes in oxygen concentration (-6 μmol kg^{-1}) and in dissolved inorganic carbon concentration (9 μmol kg^{-1}) through along-isopycnal advection (i.e., north-south lateral alongcoast advection). However, unlike the effect these processes have on salinity, large-scale intrusion events, like the intrusion of northern water during 2004, can have an effect on oxygen concentrations and on dissolved inorganic carbon concentrations similar to that of upwelling variability. During the intrusion event in 2004, oxygen concentrations increased, on average by 16 ± 6 μmol kg^{-1}, which is similar scale to the change in oxygen concentration associated with typical upwelling variability, while dissolved inorganic carbon concentrations decreased by about 25 ± 9 μmol kg^{-1}. Furthermore, the magnitude of this intrusion event is similar to the interannual variation in oxygen concentrations (12 μmol kg^{-1}) of source water that are linked to NPGO variability, as measured by Peterson et al. (2013).

Thus, it is through event-scale alongcoast advection and typical upwelling variability, including strength, vertical structure, and apparent source depth of upwelling, rather than the composition of the slope water itself, that upper slope water properties and midshelf bottom water properties are primarily connected on longer-than-seasonal scales. While on average, upwelling variability is expected to have a greater impact on oxygen and dissolved inorganic carbon concentrations than does alongcoast advection, large-scale alongcoast intrusion events can have an effect comparable to that of typical upwelling variability. This suggests that event-scale alongcoast advection and upwelling variability can have comparable effects on shelf and slope water chemistry. The precision of this conclusion is limited by a relatively short record. Future investigation into longer-term variability and trends in the northern CCS must carefully consider both the vertical structure and large-scale alongcoast transport of waters over the linked shelf-slope system.

Acknowledgments

Special thanks to Barbara Hickey for guidance and extensive help with analysis and editing, to Samantha Siedlecki, Sarah Giddings, and Ryan McCabe for useful discussions, to LuAnne Thompson and Simone Alin for guidance, and to David Darr for computer cluster administration and support. Access to model run setup files and derived output used in this paper are available upon request as described here: iodlabs.ucsd.edu/sgiddings/PNWTOX/contact.html. These model setup files and output data are curated by MacCready on MacCready's server at UW and will remain curated for at least 5 years. This work was part of H. Stone's graduate research at the University of Washington. H. Stone was supported by an Integrative Graduate Education and Research Traineeship (IGERT) grant as part of the University of Washington's IGERT Program on Ocean Change, and by a National Science Foundation (NSF) Graduate Research Fellowship. P. MacCready and N. Banas were supported by the Coastal Ocean Program of the National Oceanic and Atmospheric Administration (NA09NOS4780180) and the National Science Foundation (OCE0942675) as part of the Pacific Northwest Toxins (PNWTOX) project. In addition, N. Banas was supported by the National Aeronautics and Space Administration (NNX13AL28G). This is contribution 902 and 15 of the ECOHAB and PNWTOX programs. The findings and conclusions are those of the authors and do not necessarily reflect those of NSF, NOAA, NASA, or the Department of Commerce.

References

Alford, M. H., & MacCready, P. (2014). Flow and mixing in Juan de Fuca Canyon, Washington. *Geophysical Research Letters*, *41*, 1608–1615. https://doi.org/10.1002/2013GL058967

Banas, N. S., Conway-Cranos, L., Sutherland, D. A., MacCready, P., Kiffney, P., & Plummer, M. (2015). Patterns of river influence and connectivity among subbasins of Puget Sound, with application to bacterial and nutrient loading. *Estuaries and Coasts*, *38*, 735–753. https://doi.org/10.1007/s12237-014-9853-y

Banas, N. S., McDonald, P. S., & Armstrong, D. A. (2009). Green crab larval retention in Willapa Bay, Washington: An intensive Lagrangian modeling approach. *Estuaries and Coasts*, *32*(5), 893–905. https://doi.org/10.1007/s12237-009-9175-7

Barron, C. N., Smedstad, L. F., Dastugue, J. M., & Smedstad, O. M. (2007). Evaluation of ocean models using observed and simulated drifter trajectories: Impact of sea surface height on synthetic profiles for data assimilation. *Journal of Geophysical Research: Oceans*, *112*, C07019. https://doi.org/10.1029/2006JC003982

Battisti, D. S., & Hickey, B. M. (1984). Application of remote wind-forced coastal trapped wave theory to the Oregon and Washington Coasts. *Journal of Physical Oceanography*, *14*(5), 887–903. https://doi.org/10.1175/1520-0485(1984)014<0887:AORWFC>2.0.CO;2

Bograd, S. J., Buil, M. P., Di Lorenzo, E., Castro, C. G., Schroeder, I. D., Goericke, R.,. . . Whitney, F. A. (2015). Changes in source waters to the Southern California Bight. *Deep Sea Research, Part II*, *112*, 42-52. https://doi.org/10.1016/j.dsr2.2014.04.009

Chhak, K., & Di Lorenzo, E. (2007). Decadal variations in the California Current upwelling cells. *Geophysical Research Letters*, *34*, L14604. https://doi.org/10.1029/2007GL030203

Connolly, T. P., & Hickey, B. M. (2014). Regional impact of submarine canyons during seasonal upwelling. *Journal of Geophysical Research: Oceans*, *119*, 953–975. https://doi.org/10.1002/2013JC009452

Connolly, T. P., Hickey, B. M., Geier, S. L., & Cochlan, W. P. (2010). Processes influencing seasonal hypoxia in the northern California Current System. *Journal of Geophysical Research*, *115*, C03021. https://doi.org/10.1029/2009JC005283

Connolly, T. P., Hickey, B. M., Shulman, I., & Thomson, R. E. (2014). Coastal trapped waves, alongshore pressure gradients, and the California Undercurrent. *Journal of Physical Oceanography*, *44*(1), 319–342. https://doi.org/10.1175/JPO-D-13-095.1

Davis, K. A., Banas, N. S., Giddings, S. N., Siedlecki, S. A., MacCready, P., Lessard, E. J.,. . . Hickey, B. M. (2014). Estuary-enhanced upwelling of marine nutrients fuels coastal productivity in the U.S. Pacific Northwest. *Journal of Geophysical Research: Oceans*, *119*, 8778–8799. https://doi.org/10.1002/2014JC010248

Di Lorenzo, E., Fiechter, J., Schneider, N., Braceo, A., Miller, A. J., Franks, P. J. S.,. . . Hermann, A. J. (2009). Nutrient and salinity decadal variations in the central and eastern North Pacific. *Geophysical Research Letters*, *36*, 2003–2008. https://doi.org/10.1029/2009GL038261

Di Lorenzo, E., Schneider, N., Cobb, K. M., Franks, P. J. S., Chhak, K., Miller, A. J.,. . . Rivière, P. (2008). North Pacific Gyre Oscillation links ocean climate and ecosystem change. *Geophysical Research Letters*, *35*, L08607. https://doi.org/10.1029/2007GL032838

Egbert, G. D., & Erofeeva, S. Y. (2002). Efficient inverse modeling of Barotropic Ocean tides. *Journal of Atmospheric and Oceanic Technology*, *19*(2), 183–204. https://doi.org/10.1175/1520-0426(2002)019<0183:EIMOBO>2.0.CO;2

Emery, W. J., & Thomson, R. E. (2004). *Data analysis methods in physical oceanography* (2nd ed., 638 p.). Amsterdam: Elsevier.

Feely, R., & Sabine, C. (2011). *Carbon dioxide and hydrographic measurements during the 2007 NACP West Coast Cruise*. Oak Ridge, TN: Carbon Dioxide Information Analysis Center, Oak Ridge National Laboratory, US Department of Energy. Retrieved fromhttp://cdiac.ornl.gov/ftp/oceans/NACP_West_Coast_Cruise_2007/; https://doi.org/10.3334/CDIAC/otg.CLIVAR_NACP_West_Coast_Cruise_2007

Freeland, H. J., Gatien, G., Huyer, A., & Smith, R. L. (2003). Cold halocline in the northern California Current: An invasion of subarctic water. *Geophysical Research Letters*, *30*(3), 1141. https://doi.org/10.1029/2002GL016663

Garcia, H. E., Locarnini, R. A., Boyer, T. P., Antonov, J. I., Baranova, O. K., Zweng, M. M.,. . . Johnson, D. R. (2014). World Ocean Atlas 2013, Volume 3: Dissolved oxygen, apparent oxygen utilization, and oxygen saturation. In S. Levitus & A. Mishonov (Eds.), *NOAA Atlas* (NESDIS 75, 27 pp.). Silver Spring, MD: National Oceanic and Atmospheric Administration.

Giddings, S. N., MacCready, P., Hickey, B. M., Banas, N. S., Davis, K. A., Siedlecki, S. A.,. . . Connolly, T. P. (2014). Hindcasts of potential harmful algal bloom transport pathways on the Pacific Northwest coast. *Journal of Geophysical Research: Oceans*, *119*, 2439–2461. https://doi.org/10.1002/2013JC009622

Grantham, B. A., Chan, F., Nielsen, K. J., Fox, D. S., Barth, J. A., Huyer, A.,. . . Menge, B. A. (2004). Upwelling-driven nearshore hypoxia signals ecosystem and oceanographic changes in the northeast Pacific. *Nature*, *429*(June), 749–754. https://doi.org/10.1038/nature02605

Hickey, B. M. (1979). The California current system-hypotheses and facts. *Progress in Oceanography*, *8*(4), 191–279. https://doi.org/10.1016/0079-6611(79)90002-8

Hickey, B. M. (1989). Patterns and processes of circulation over the Washington continental shelf and slope. In *Coastal oceanography of Washington and Oregon* (pp. 41–115). Amsterdam, Netherlands: Elsevier Science Publishers B.V.

Hickey, B. M. (1997). The response of a steep-sided, narrow canyon to time-variable wind forcing. *Journal of Physical Oceanography*, *27*(5), 697–726. https://doi.org/10.1175/1520-0485(1997)027<0697:TROASS>2.0.CO;2

Hickey, B. M., & Banas, N. S. (2003). Oceanography of the U.S. Pacific Northwest coastal ocean and estuaries with application to coastal ecology. *Estuaries*, *26*(4), 1010–1031. https://doi.org/10.1007/BF02803360

Hickey, B. M., Geier, S., Kachel, N., Ramp, S., Kosro, M., & Connolly, T. P. (2016). Alongcoast structure and interannual variability of seasonal midshelf water properties and velocity in the Northern California Current System. *Journal of Geophysical Research: Oceans*, *121*, 7408–7430. https://doi.org/10.1002/2015JC011424

Hickey, B., MacFadyen, A., Cochlan, W., Kudela, R., Bruland, K., & Trick, C. (2006). Evolution of chemical, biological, and physical water properties in the northern California Current in 2005: Remote or local wind forcing? *Geophysical Research Letters*, *33*, L22S02. https://doi.org/10.1029/2006GL026782

Huyer, A. (1977). Seasonal variation in temperature, salinity, and density over the continental shelf off Oregon. *Limnology and Oceanography*, *22*, 442–453.

Huyer, A. (2003). Preface to special section on enhanced Subarctic influence in the California Current, 2002. *Geophysical Research Letters*, *30*(15), 8019. https://doi.org/10.1029/2003GL017724

Huyer, A., & Smith, R. L. (1985). The signature of El Niño off Oregon, 1982–1983. *Journal of Geophysical Research*, *90*(C4), 7133. https://doi.org/10.1029/JC090iC04p07133

Jacox, M. G., Fiechter, J., Moore, A. M., & Edwards, C. A. (2015). ENSO and the California Current coastal upwelling response. *Journal of Geophysical Research: Oceans*, *120*, 1691–1702. https://doi.org/10.1002/2014JC010650

Keister, J. E., Di Lorenzo, E., Morgan, C. A., Combes, V., & Peterson, W. T. (2011). Zooplankton species composition is linked to ocean transport in the Northern California Current. *Global Change Biology*, *17*(7), 2498–2511. https://doi.org/10.1111/j.1365-2486.2010.02383.x

Kosro, P. M. (2002). A poleward jet and an equatorward undercurrent observed off Oregon and northern California, during the 1997–98 El Niño. *Progress in Oceanography*, *54*(1–4), 343–360. https://doi.org/10.1016/S0079-6611(02)00057-5

Kosro, P. M. (2003). Enhanced southward flow over the Oregon shelf in 2002: A conduit for subarctic water. *Geophysical Research Letters*, *30*(15), 8023. https://doi.org/10.1029/2003GL017436

Lentz, S. J. (1992). The surface boundary layer in coastal upwelling regions. *Journal of Physical Oceanography*, *22*, 1517–1539. https://doi.org/10.1175/1520-0485(1992)022<1517:TSBLIC>2.0.CO;2

MacFadyen, A., Hickey, B. M., & Cochlan, W. P. (2008). Influences of the Juan de Fuca Eddy on circulation, nutrients, and phytoplankton production in the northern California Current System. *Journal of Geophysical Research: Oceans*, *113*, C08008. https://doi.org/10.1029/2007JC004412

Mass, C. F., Albright, M., Ovens, D., Steed, R., MacIver, M., Grimit, E.,. . . Brown, W. (2003). Regional environmental prediction over the Pacific Northwest. *Bulletin of the American Meteorological Society*, *84*(10), 1353–1366, 1328. https://doi.org/10.1175/BAMS-84-10-1353

McCabe, R. M., Hickey, B. M., Dever, E. P., & MacCready, P. (2015). Seasonal cross-shelf flow structure, upwelling relaxation, and the alongshelf pressure gradient in the Northern California Current System. *American Meteorological Society*, *45*, 209–227. https://doi.org/10.1175/JPO-D-14-0025.1

Meinvielle, M., & Johnson, G. C. (2013). Decadal water-property trends in the California Undercurrent, with implications for ocean acidification. *Journal of Geophysical Research: Oceans*, *118*, 6687–6703. https://doi.org/10.1002/2013JC009299

Nelder, J., & Wedderburn, R. (1972). Generalized linear models. *Journal of the Royal Statistical Society. Series A*, *135*(3), 370–384.

Pelland, N. A., Eriksen, C. C., & Lee, C. M. (2013). Subthermocline eddies over the Washington continental slope as observed by seagliders, 2003–09. *Journal of Physical Oceanography*, *43*(10), 2025–2053. https://doi.org/10.1175/JPO-D-12-086.1

Peterson, J. O., Morgan, C. A., Peterson, W. T., & Di Lorenzo, E. (2013). Seasonal and interannual variation in the extent of hypoxia in the northern California Current from 1998–2012. *Limnology and Oceanography*, *58*(6), 2279–2292. https://doi.org/10.4319/lo.2013.58.6.2279

Pierce, S. D., Barth, J. A., Shearman, R. K., & Erofeev, A. Y. (2012). Declining oxygen in the Northeast Pacific. *Journal of Physical Oceanography*, *42*(3), 495–501. https://doi.org/10.1175/JPO-D-11-0170.1

Pierce, S. D., Barth, J. A., Thomas, R. E., & Fleischer, G. W. (2006). Anomalously warm July 2005 in the northern California Current: Historical context and the significance of cumulative wind stress. *Geophysical Research Letters*, *33*, L22S04. https://doi.org/10.1029/2006GL027149

Pierce, S. D., Smith, R. L., Kosro, P. M., Barth, J. A., & Wilson, C. D. (2000). Continuity of the poleward undercurrent along the eastern boundary of the mid-latitude north Pacific. *Deep Sea Research, Part II*, *47*(5–6), 811–829. https://doi.org/10.1016/S0967-0645(99)00128-9

Rivas, D., & Samelson, R. M. (2011). A numerical modeling study of the upwelling source waters along the Oregon coast during 2005. *Journal of Physical Oceanography*, *41*(1), 88–112. https://doi.org/10.1175/2010JPO4327.1

Schwing, F. B., Murphree, T., DeWitt, L., & Green, P. M. (2002). The evolution of oceanic and atmospheric anomalies in the northeast Pacific during the El Niño and La Niña events of 1995–2001. *Progress in Oceanography*, *54*(1–4), 459–491. https://doi.org/10.1016/S0079-6611(02)00064-2

Shchepetkin, A. F., & McWilliams, J. C. (2005). The regional oceanic modeling system (ROMS): A split-explicit, free-surface, topography-following-coordinate oceanic model. *Ocean Modelling*, *9*(4), 347–404. https://doi.org/10.1016/j.ocemod.2004.08.002

Siedlecki, S. A., Banas, N. S., Davis, K. A., Giddings, S., Hickey, B. M., MacCready, P.,. . . Geier, S. (2015). Seasonal and interannual oxygen variability on the Washington and Oregon continental shelves. *Journal of Geophysical Research: Oceans*, *120*, 608–633. https://doi.org/10.1002/2014JC010254

Sutherland, D. A., MacCready, P., Banas, N. S., & Smedstad, L. F. (2011). A model study of the Salish Sea Estuarine Circulation. *Journal of Physical Oceanography*, *41*(6), 1125–1143. https://doi.org/10.1175/2011JPO4540.1

Thomson, R. E., & Krassovski, M. V. (2010). Poleward reach of the California Undercurrent extension. *Journal of Geophysical Research*, *115*, C09027. https://doi.org/10.1029/2010JC006280

Tinis, S. W., Thomson, R. E., Mass, C. F., & Hickey, B. M. (2006). Comparison of MM5 and meteorological buoy winds from British Columbia to Northern California. *Atmosphere Ocean*, *44*(1), 65–81. https://doi.org/10.3137/ao.440105

Visser, A. (1997). Using random walk models to simulate the vertical distribution of particles in a turbulent water column. *Marine Ecology Progress Series*, *158*, 275–281. https://doi.org/10.3354/meps158275

Willmott, C. J. (1982). Some comments on the evaluation of model performance. *Bulletin of the American Meteorological Society*, *63*, 1309–1313. https://doi.org/10.1175/1520-0477(1982)063<1309:SCOTEO>2.0.CO;2